Memoirs of the Faculty of Engineering, Nagoya University
Vol. 35, No. 2 (1983)

RECENT STUDIES ON ELECTRICAL BREAKDOWN IN POLYMERS

MASAYUKI IEDA and MASAYUKI HIKITA

Department of Electrical Engineering

(Received Octoer 26, 1983)

Abstract

Much experimental work has been done on the electrical breakdown of solid dielectrics, and a number oh breakdown theories have been proposed. Many problems, however, still remain on the breakdown process of polymers. Here, the breakdown processes of polymers are discussed from the standpoint of the inherent properties of polymers such as chemical structure, structural irregularities, the presence of additives, molecular motion and so on.

Further, as for the long-term breakdown processes of polymer insulation systems, electrical degradations caused by partial discharge and treeing breakdown have been mentioned as important factors.

Using experimental results obtained in our laboratory together with those presented by others, our considerations on fundamental processes of electrical degradation are reported. Also, the behavior of dc trees caused by space charge accumulation is discussed with the nature of carrier injection and trapping in polymers, which is estimated by thermally stimulated current and thermoluminescence measurements.

CONTENTS

1. Introduction

1. 1. Introduction

Much experimental work has been done on the electrical breakdown of solid dielectrics[1, 2] and a number of breakdown theories have also been proposed[3]. Many problems, however, still remain for fully understanding the breakdown process of polymers. The electrical breakdown processes of various kinds of polymers will be discussed in Chapter 2 from the standpoint of properties inherent to polymers such as chemical structure, structural irregularities, additives, molecular motion and so on. Chapter 3 deals with space charge as one of the secondary factors conrolling the breakdown process with practical examples. Also, the fundamental process of electrical treeing breakdown will be discussed.

1. 2. Typical Characteristics of Electrical Breakdown Phenomena in Polymers

1. 2. 1. Electrical Breakdown Strength

The measured values of the breakdown voltage V_B of solid dielectrics are greatly influenced by the experimental conditions. For instance, when voltage is applied to the solid specimen kept in a surrounding medium of liquid or gas, a partial discharge in the surounding medium often occurs mainly at the edge of the electrode before a complete breakdown of the solid dielectric. This phenomenon decreases V_B of solids. This is called the edge effect. In order to eliminate this effect, special forms of specimens and electrodes have been developed.[4~8] If electric strength F_B ($=V_B$/sample thickness) is measured carefully with dc voltage eliminating the edge effect, the following features are commonly observed for polymers.

(a) The electric strengths of polymers are generally in the range of 1 to 9 MV/cm (at 20℃) and these values are higher than those of ionic crystals (0.5 to 1 MV/cm at 20℃).

(b) In general, the maximum values of the electric strengths of polymers are obtained in the low temperature region. These values for polar polymers excede 10 MV/cm and are higher than those of nonpolar polymers.

(c) The highest electric strength so far obtained for polymers is 15 MV/cm at −190℃ for polyvinyl alcohol, having a polar group (−OH) in its side chain.

1. 2. 2. Temperature Dependence

Physical properties of polymers change with temperature, so the temperature dependence of their dielectric breakdown is of prime importance in analyzing their breakdown mechanisms. In general, the temperature dependence of F_B of polymers is roughly divided into the following two regions.

(a) Low temperature region: $\partial F_B/\partial T \approx 0$ (T=temperature) In this region F_B increases slightly with increasing temperature or F_B is almost independent of

Table 1. Structural and morphological features of typical polymers.

Polymer	Structural unit			Features *	Features **
	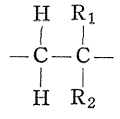	R_1	R_2		
Polyethylene (PE)					
low density (LDPE)		H	H	N	C
high density (HDPE)				N	C
Polystyrene (PS) (atactic)		H	C_6H_5	N	A
Polypropylene (PP)					
atactic (a-PP)		H	CCH_3	N	A
isotactic (i-PP)				N	C
Ethylene-propylene copolymer (E-P)		H	H CH_3	N	A
Polyisobutylene (PIB)		CH_3	CH_3	N	A
Polyvinyl alcohl (PVAl)		H	OH	P	C
Polyvinyl chloride (PVC)		H	Cl	P	A
Polymethyl methacrylate (PMMA)		CH_3	$COOCH_3$	P	A
Polyvinyl chloride-asetate copolymer (PVC-AC)		H	Cl $OCOCH_3$	P	A
Ethylene-vinyl asetate copolymer (EVA)		H	H $OCOCH_3$	P	C(A)
Polyvinydene-fluoride (PVDF)		F	F	P	C
Polybutadiene (PBD)	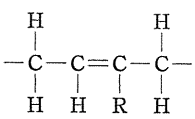		R H	N	A
Poly 1, 4-cis isoprene (NR)			CH_3	N	A
Nylon 6 (N6)	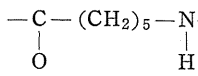			P	C
Polyethylene terephthalate (PET)	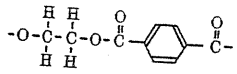			P	C, A
Polycarbonate (PC)	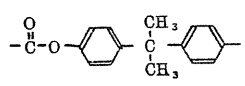			P	C
Polyimide (PI)	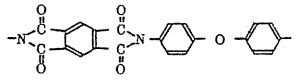			P	A
Polyamideimide (PAI)	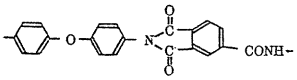			P	A

* P: polar, N: nonpolar ** C: crystalline, A: amorphous

temperature.

(b) High temperature region: $\partial F_B/\partial T<0$ In this region, F_B decreases with rising temperature.

Figures 1 (a) and (b) show the temperature dependence of F_B for various polymers listed in Table 1. The breakdown characteristics shown in Fig. 1 are

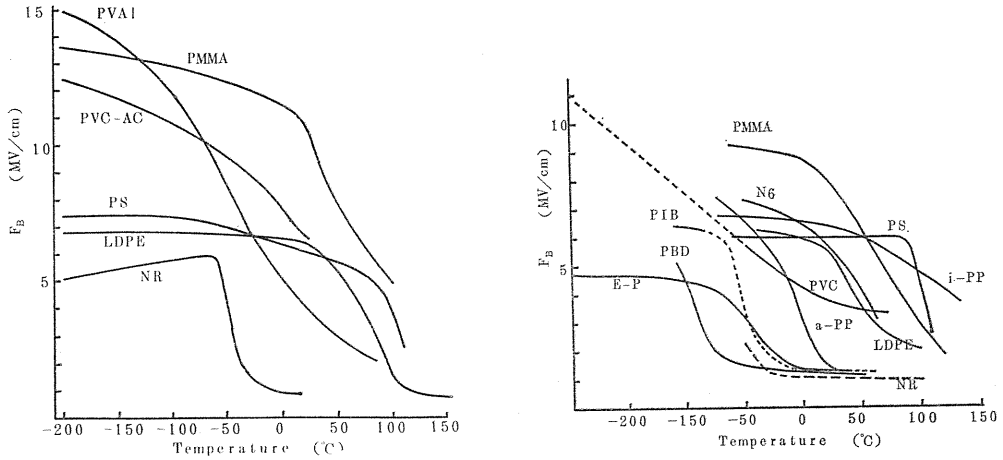

Fig. 1. Examples of the temperature dependence of eleactric strength of polymers with recessed specimens and dc voltage.

classified into two types. For nonpolar polymers, there clearly exist the low and the high temperature regions. For polar polymers, however, as temperature rises, F_B decreases from an extremely low temperature (−200℃) to some critical temperature (T_c) from which F_B falls steeply. Thus, there does not exist a clear low temperature region for polar polymers.

1. 2. 3. Time Dependence

In general, electrical breakdown occurs at a time after the voltage appliaction. This time delay for the breakdown varies from a very short value, about 10^{-9}sec, to a very long one, longer than several hours, depending on the breakdown mechanism.

For the short time delays where the electrical breakdown in mainly caused by the electronic processes, this time delay is called time lag and shows statistical features like in gaseous breakdowns. Usually, the time lag consists of the statistical time lag t_s and the formative time lag t_f. For the distribution of the observed time lag t, the following relation has been derived[14]

$$N(t)/N_0=\exp\{-(t-t_f)/\overline{t_s}\} \tag{1}$$

where $N(t)$ is the number of the experiments in which breakdown does not take place before the time t in a series of N_0 experiments under the same conditions, $\overline{t_s}$ is the mean statistical time lag (this is also called the statistical time lag), and t_f is assumed to be constant for a given electric field. Fig. 2 shows an example of

the Laue plot of the time lag ($\ln (N(t)/N_0)$ vs. t) for the electrical breakdown of polyethylene in the low temperature region[15]. The statistical time lag estimated from the slope of a linear graph of the Laue polt varies with the applied electric field and the electrode materials.

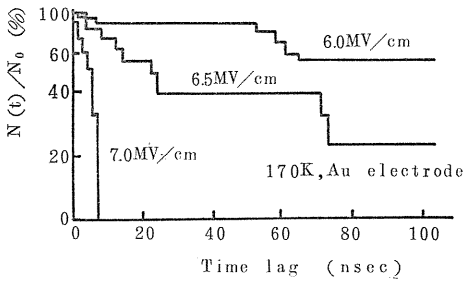

Fig. 2. Laue polt of time lag in electrical breakdown of polyethylene.[15]

1. 3. Electrical Breakdown Mechanism

1. 3. 1. Historical Survey

The first breakdown theory of solid dielectrics was the thermal breakdown theory presented by Wagner in 1922.[16] in this theory, the electrical breakdown was discussed in terms of the condition to lose the thermal balance between Joule heating due to the conduction current and its dissipation. This theory succeeded in explaining qualitatively the electrical breakdown phenomena of the practical apparatuses and devices in the high temperature region ($\partial F_B/\partial T<0$).

However, it was difficult to explain the electrical breakdown phenomena in the low temperature region by the thermal breakdown theory. This led to the recognition of the existence of the electronic conduction current in solid dielectrics. The investigations of time lag[17], the direction of the breakdown path[18] and other successive studies[2,3] suggested that the electrical breakdown of solids are also due to an electronic process such as the current multiplication by collision ionization of high speed electrons as in gases. Thus, the electronic process was identified as playing an important role in some breakdown processes. For example, the interactions between hot electrons accelerated by the applied electric field and phonons attracted much interest as a subject of theoretical physics in 1940 to 1950. These theories dealt quantitatively with the quantum mechanical solid state physics, and the breakdown mechanism was understood mainly for the alkali halide single crystals whose structure is relatively simple. Within this framework, a number of different breakdown theories were presented according to differences in the approximation and the energy exchange processes, but the agreement between the theories and the experimental results was not satisfactory. This was partly because the theories included unknown basic quantities and partly because many secondary effects could not always be eliminated in the experiments.

On the other hand, the breakdown characteristics in the high temperature region have been explained for a long time only by the thermal breakdown theory. The investigation of time lag for the breakdown suggested that the thermal breakdown was not the only breakdown process in this region. Proposals were made to modify the collision ionization of electrons with the space charge effect[19,20] and to consider what role the interaction between the conduction electrons and the electrons trapped in the impurity level plays in the energy exchange process (Fröhlich's amorphous theory[21]). Further, on the basis of the fact that the breakdown characteristics of polymers in the temperature region near the melting (or softening)

point are similar to their mechanical characteristics, the electromechanical breakdown theory[22] was proposed. This states that the breakdown is caused by the mechanical deformation due to Maxwell stress under the applied electric field. This theory was inherent to polymers and succeeded in explaining the breakdown characteristics of many polymers in the high temperature region. Another breakdown theory inherent to polymers was the free volume breakdown theory presented by Artbauer,[23] which was taken in explaining the breakdown phenomena of polymers around the glass transition temperature region.

Though many breakdown theories have been proposed, it is still difficult to decide which mechanism plays a dominant role in the breakdown phenomena. This is the reason why the checks from various directions are desired in order to clarify the breakdown mechanism. Among all the theories mentioned above, thermal breakdown theory has most developed because of an easiness of analyses. The steady-state thermal breakdown, where the time dependent term is neglected in the equation governing thermal breakdown, was treated analytically by Wintel[24], Moon[25], O'Dwyer[3] and Klein.[26] Hikita et al.[27] gave a general method to solve numerically the equations of the steady-state thermal breakdown for a field dependent conductivity. Vermeer[28] applied the impulse thermal breakdown theory, which neglects the heat conduction term, to explain the experimental breakdown date for glass. Also, Miyairi et al.[29] for impurity-doped polythylene, Hikita et al.[30, 31] for poly (vinyliden-fluoride) and Miyairi[32] for poly (ethylene-terephthalate) employed the impulse thermal theory. O'Dwyer[33] and Copple et al.[34] numericallly solved the fundamental equation of thermal breakdown in one dimension. Hikita et al.[35, 36] numerically solved the fundamental equation of thermal breakdown under the boundary condition which obeys Newton's law of cooling for various values of heat transfer coefficient from the dielectric surface to the ambient. It was found that the impulse thermal assumption is valid even if the thermal time constant of dielectric is shorter than the voltage duration to breakdown, provided the heat transfer coefficient is smaller than a critical value.

1. 3. 2. Summary of Breakdown Theories

Some facts must be kept in mind in developing breakdown theories. In general, the electrical breakdown of solids is observed accompanying the destruction of the molecular structure which leads to the transition to conductive material. At this time the current multiplication occurs very rapidly. In order to construct the breakdown theory, we must find at first what the charge carriers are and what the multipication process is, and then introduce the brakdown condition into it.

In this point of view, the fundamental breakdown processes are roughly classified into the electronic process and the pure thermal process. Further, regardless of the current multiplication process, there exists the mechanical breakdown process, in which the mechanical deformation under the applied electrical field dominates the breakdown phenomena. The summary of the breakdown mechanisms is shown in Table 2.

When the electric field is applied to the sample, the electrical breakdown is considered to occur at the minimum value among the electric strengths given by each theory. However, it is usually difficult to interpret the breakdown phenomena in solid dielectrics, especially such as polymers, by a single breakdown mechanism Carrier injection process from the electrode, bulk conduction and various secondary effects such as space charge, local heating and Maxwell stress should be taken into

Table 2. Dielectric Breakdown Theories of Solids.

I. Electronic breakdown process
- Intrinsic breakdown ($\partial F_B/\partial d=0$), d: sample thickness
  - Theories based on the single electron approximations ($\partial F_B/\partial T \geqq 0$)
    - High energy criterion
    - Low energy criterion
  - Collective critical field theories
    - Single crystal ($\partial F_B/\partial T>0$)
    - Amorphous materials ($\partial F_B/\partial T<0$)
- Electron avalanche breakdown ($\partial F_B/\partial d<0$) ($\partial F_B/\partial T \geqq 0$)
  - Single avalanche model
  - Collective avalanche model
- Field emission breakdown ($\partial F_B/\partial d=0$) ($\partial F_B/\partial T=0$)
- Free volume breakdown ($\partial F_B/\partial T<0$)

II. Thermal breakdown process
- Steady state thermal breakdown ($\partial F_B/\partial T<0$)
- Impulse thermal breakdown

III. Mechanical breakdown process
- Electromechanical breakdown ($\partial F_B/\partial T<0$)

considaration in a practical breakdown model. There are two alternative ways to construct the breakdown model. The first way is that the various effects and processes are regarded as secondary effects for a basic single breakdown mechanism. The second is that all the considerable processes are included in the breakdown model as multi-step breakdown processes. It is thought that the second way is better than the first in a sense of understanding the relation between the theory and the experiment quantitatively.

2. Fundamental Breakdown Phenomena of Polymers

Many problems still remain with respect to the electrical breakdown processes of polymers which exhibit highly complex structures. In order to solve these problems, it is necessary to clarify the relation between the electrical breakdown phenomena and the properties inherent to polymers such as chemical structure, molecular motion, structural irregularities, and existence of additives and so on.

In this Chapter, fundamental electrical breakdown of polyethylene (PE), polyimide (PI), polyamideimide (PAI), poly (vinylidene-fluoride) (PVDF), and plasma polymerized styrene thin film(PPS) are discussed in turn.

2. 1. Electrical Breakdown of Polyethylene

Many reports on the electrical breakdown of polyethylene (PE) have so far been published.[1] The essential feature of the temperature dependence of the electric strength F_B of PE is schematically given in Fig. 3.[1] The temperature

range can be classified into three parts: Regions Ⅰ, Ⅱ, and Ⅲ. The lower critical temperature T_{c1}, which is ranged from −40 to −100℃, is closely related to glass transition temperature and the upper critical temperature T_{c2} is related to the temperature at which crystalline part begin to melt. Corresponding to each region, the rheology of PE and the possible breakdown processes are summarized in Table 3. These descriptions are based on the consideration of various factors listed in Table 4.

In this section, the breakdown mechanism of PE in each region will be discussed, focussing attention on the relation

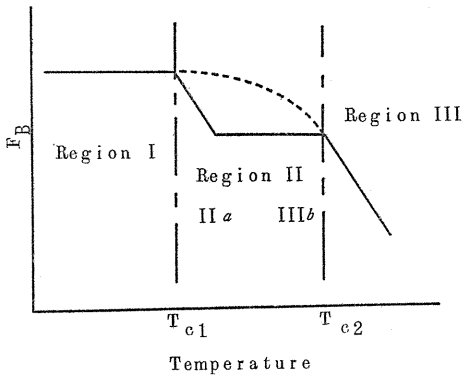

Fig. 3. Outline of the temperature dependence of electric strength of PE.

Table 3. Corresponding Breakdown Processes for Regions Ⅰ, Ⅱ and Ⅲ inFig. 3.

Region	Molecular state	Corresponding breakdown process
Ⅰ	Glass-like	Electron avalanche breakdown
Ⅱ	Rubber-like	a) Collective breakdown for amorphous dielectrics b) Thermal breakdown c) Free volume breakdown
Ⅲ	Plastic-flow	a) Thermal breakdown b) Electromechanical breakdown

* Secondary effects: Space charge, Local heating, Maxwell stress and so on.

Table 4. Various factors affecting F_B of PE.

Factor		Electric strength		
		Region		
		Ⅰ	Ⅱ	Ⅲ
Introducing polar molecules		+	?	?
Increasing molecular weight		*	+	+
Cross-linking		?	?	+
Increasing crystallinity		−	?	+
Impurity	with rich π electrons	+	*	*
	which decreases specimen resistivity	*	−	−

Symbols in the table mean: +: "increase", −: "decrease", *: "not so sensitive", ? : "unknown or complicated".

between the electrical breakdown and the polymer morphology, additives and so on.

2. 1. 1. Low Temperature Region (Region I)

In Region I, molecular state of PE is glass-like as micorbrownian motion of molecular chains in amorphous parts is frozen. It was already reported that in low temperature region F_B scarcely varies with temperature[4, 5, 10, 13, 37] and increases with introducing polar group,[11,38~41] and impurity with rich π electrons[42] and also with decreasing crystallinity.[13, 37] From these results, as well as that on the time lag,[15] the electron avalanche breakdown process is thought dominant in this region. In this section, we will discuss the breakdown mechanism in low temperature region in more details with respect to the data on the effect of crystallinity,[4, 37] an introduction of polar group,[38, 40, 41] and impurity with π electrons on the breakdown which are obtained in our labolatory.

(1) *Crystallinity*

(ii) *Specimens and Experimental Procedures*

Materials used were low-density and high-density PE (abbreviated LDPE and HDPE, respectively) which were free of additives. Their physical properties are given in Table 5. In order to investigate the effect of crystallite on F_B in Region I, ethylene-vinyl acetate copolymers (EVA) and their blends with LDPE were also used. Their vinyl acetrate content (VA wt. %) and the composition of the blended materials are listed in Table 6. The thickness of the film specimen is about 20~30 μm. Electrodes were applied on both sides by vacuum deposition of gold with diffused edges for preventing the field localization as shown in Fig. 4.

Table 5. Sample description.

	LDPE (Yukalon LK-30)	HDPE (Yukalon PX-40)
Melt index	4	1.6
Melting point	115℃	135℃
Density	0.925g/cm^3	0.960g/cm^3
Crystallinity	46~47%	82~84%

Table 6. Sample description.

	Vinyl acetate content wt. %	Composition
LDPE	0	homopolymer
EVA-1	5.5	copolymer
EVA-2	16.5	copolymer
EVA-3	22.0	copolymer
BLEND-1	5.5	blend: 25%EVA-3+75%LDPE
BLEND-2	16.5	blend: 75%EVA-3+25%LDPE

The specimen was mounted between a brass-ball and a brass-plate in a suitable insulating liquid: liquid nitrogen at −196 ℃ and silicone oil at the other temperatures. Values of electric strength were obtained with either a direct voltage or a rectangular pulse voltage. Unless otherwise noted, the direct voltage was increased at a rising rate of 500V/sec and the amplitude of successive pulses of about 0.2 μsec in rise time and 5μ sec in width was increased by a step of 50V/pulse at a repetition rate of 10/sec.

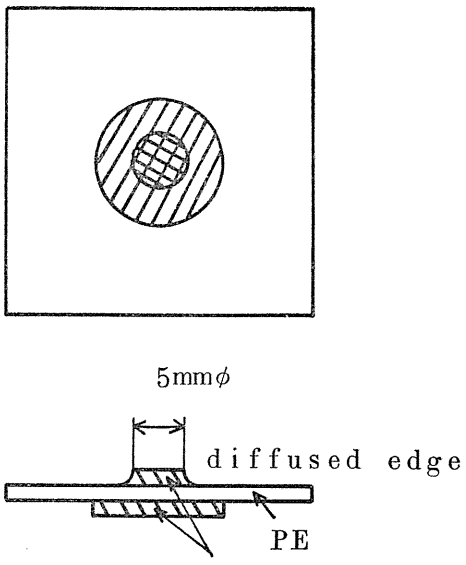

Fig. 4. Specimens.

(ii) *Results and Discussion*

The electric strength F_B obtained with the film specimens are shown in Fig. 5. The results were accepted only when the breakdown occurred within the upper evaporated electrode. Each point represents a mean value of about twenty tests. As shown in the figure, in the low temperature region below about −50℃ F_B

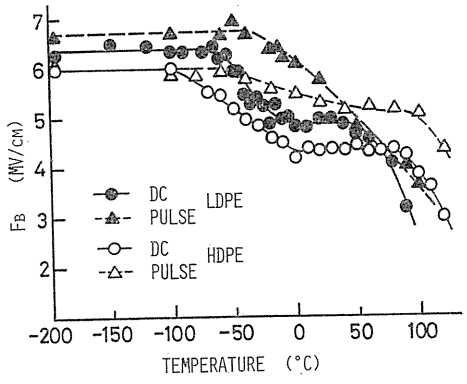

Fig. 5. The temperature dependence of F_B of PE film with the dc and pulse voltage.

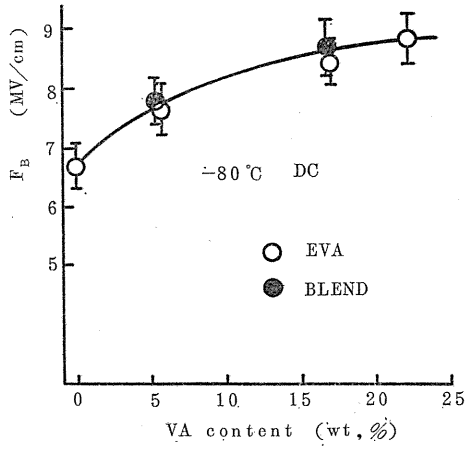

Fig. 6 F_B of polyethylene, ethylene vinyl acetate copolymer and their blend as function of VA wt.% at −80℃.

of both samples HDPE and LDPE scarcely varies with temperature. It is also seen that HDPE gives a lower value of F_B than LDPE for both modes of stress. It follows that F_B decreases with increasing crystallinity. This can be interpreted in terms of the avalanche process if the ionization coefficient is higher in the crystalline part than in the amorphous part as would be anticipated.

F_B is shown as a function of VA wt.% in Fig. 6. It can be seen that F_B rises as the amount of VA wt. % increases. The incorporation of vinyl acetate comonomer units into a backbone chain has two separate effects: one is the reduction of crystallinity and the other is an introduction of polar group.[43] The experimental result mentioned above can be thus easily understood in terms of the increase of electron scattering associated with the decrease of crystallinity and the introduction of polar group.[10, 13, 41]

The comparison between copolymers and blends would infer a knowledge as to a role of crystallite on the breakdown process. As is evident from Fig. 6, the blend gives almost the same electric strength as that of the copolymer at each VA wt. %. It can be expected that both copolymer and blend have almost the same crystallinity if they have the same value of VA wt. % as a whole, but the structure and size of crystallite would be different. Figure 7 shows the melting characteristics obtained with the differential scanning calorimeter (DSC) at a heating rate of 10℃/min from samples of 5 mg in weight, where the base line is shifted for convenience. The sharp rise indicates the melting point. On comparison of LDPE, EVA-2, and EVA-3, it may be noted that the size of crystallite decreases with copolymerization since the melting point of copolymer falls with increasing VA wt. %.[43] On the other hand, two peaks, which correspond to constituent polymers, appear on the DSC curve for BLEND-2. Therefore, the blend has a crystallinity which is determined by VA wt. % as a whole, but is quite different in the nature of crystallite from copolymer. Nevertheless, the copolymer and the blend give almost the same F_B if VA wt. % is fixed. This result shows that F_B in the low temperature region is not influenced by the nature of individual micro-crystallites but by the degree of crystallinity i. e. the total amount of crystallite.

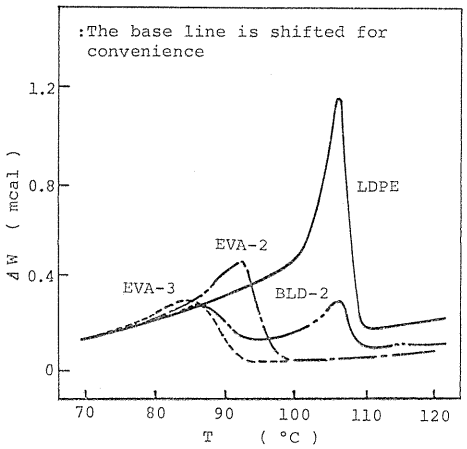

Fig. 7. Melting characteristics obtained with DSC at a heating rate of 10 ℃/min from a sample of 5 mg in weight.

It has been reported that the statistical time lag of electric breakdown of PE in the low temperature region depends on the cathode material, suggesting that a single avalanche process is operative.[15] Since the vinyl acetate unit is extruded from the crystalline part, the average content of vinyl acetate in the amorphous part is not different at a certain value of VA wt. % between the copolymer and the blend. In the single avalanche theory,[3] the critical ionization number i is given as

$$\alpha_c d_c + \alpha_a d_a = 1 \tag{2}$$

where α_c and α_a are the critical collision ionization rates per unit length in crystalline- and amorphous-part, respectively and d_c and d_a are the corresponding breakdown path length, which would depend on the total crystallinity but not on

the individual crystalline size. The present experimental result thus supports a single avalanche process in the electrical breakdown of PE in the low temperature region.

(2) *Additive (Impurities)*

Table 7. Properties of base PE and additives.

Base resin	Low-density polyethylene (Eucaron EH 30) 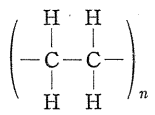	Density Melt index	0.919g/cm³ 2
Additive	Pyrene ($C_{16}H_{10}$) 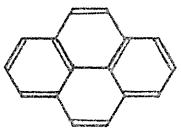	Molecular weight Density Melting point Boiling point	202 1.277g/cm³ 140℃ 404℃
	Anti-static agent (AS-1) 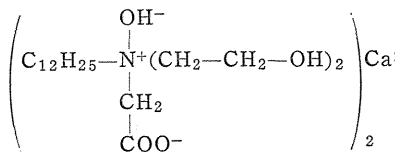	Molecular weight density Melting point	736 0.943g/cm³ 0~5℃

Various residual catalysts and the additives in polymers are some of the possible impurities. Their properties and the state of dispersion have a great influence on F_B. Base resin and doped impurities used in the experimets are listed in Table 7. The dependence of F_B on concentration of the doped impurity at −196℃ is shown in Fig. 8. Pyrene, which has a number of π electrons in its molecular structure and makes a molecular dispersion, raises F_B at low temperature. This is considered as being due to energy absorption through the interaction with the accelerated electrons.

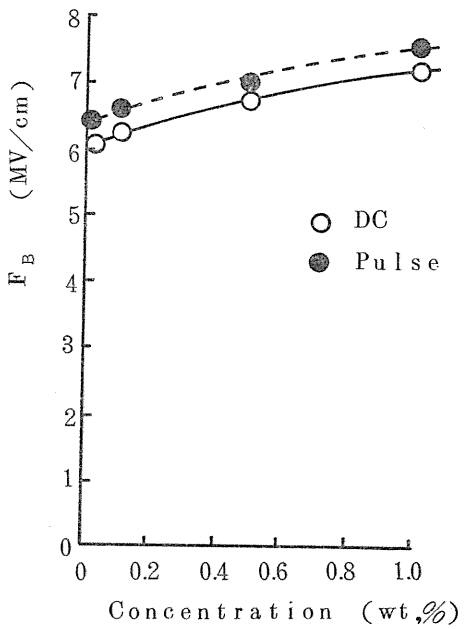

Fig. 8. Influence of pyrene on F_B of PE at −196℃.

2. 1. 2. Intermediate Temperature Region (Region Ⅱ)

In Region Ⅱ, microbrownian motion of molecular chains in amorphous parts is released, and the amorphous parts are rubberlike. In this region, Fröhlich's original amorphous breakdown theory[11, 13, 44] and its modified theory,[45] the electron avalanche theory[46~48] and the free volume breakdown theory[2, 23] are suggested to be applicable.

So far many experimental results have been taken in an attempt to elucidate the correlation between F_B and the inherent nature of PE, such as polymer morphology,[47~53] molecular motion,[4, 37] internal strain,[51, 54, 55] presence of additives [47, 56] and cross-linking[57] etc. In this section, the breakdown mechanism of PE in Region Ⅱ will be discussed, focussing attention on the data obtained in our laboratory.

(1) *Molecular Motion*

The molecular motion of polymers changes with temperature. As the temperature rises, polymers successively show glass-like, rubber-like and plastic-flow states. A characteristic molecular motion exists in each state. As shown in Table 3. the electron avalanche breakdown process and the electromechanical breakdown process are considered to be dominant in glass-like and plastic-flow states, respectively. Pay special attention to the glass transition temperature (T_g) region in Fig. 5 which shows the temperature dependence of F_B of PE. As the temperature rises, F_B sharply decreases for dc voltage around T_g and F_B of HDPE begins to fall at lower temperature than that of LDPE. Further, F_B for pulse voltage begins to decrease at higher temperature than that for dc voltage. These results suggest that the released segmental molecular motion and/or the increased rearrangement of free volumes enhance the electron transport in the amorphous region and facilitate the occurrence of the electron avalanche breakdown.

(2) *Polymer Morphology*

It is reported that F_B of PE below room temperature falls with increasing crystallinity.[13, 37, 45, 47, 58] In addition, F_B of a hexatriacontane single crystal has recently been reported to be much lower than that of conventional PE film.[59, 60] These facts suggest that the electron avalanche develops more easily in the crystalline part than in the amorphous part. On the other hand, the treeing channel has been observed to develop along boundaries between spherulites.[61] It is difficult to clarify the correlation between the electrical breakdown process and the morphology of semicrystalline polymers, since the spherulites and their boundaries usually exist in series across bulk material between the electrodes.

In this subsection, PE thin film consisting of two-dimensional spherulites is prepared in an attempt to make the spherulites and their boundaries in parallel between the electrodes, and the electrical breakdown is studied by making use of self-healing breakdown.[62]

(i) *Experimental Procedure*

The film-forming polymer was HDPE (PX-40) supplied by Mitsubishi Petrochemical Industries Co. Ltd. which had a density of 0.960g/cm^3 and a melt index of 1.6. The solvent used was xylene of reagent grade, which was further distilled twice. The polymer was also further purified in such a manner that it was dissolved in the xylene and filtered through glass fiber cloth. A few drops of the

xylene solution at various concentrations around 1 wt. % was laid down on a glass plate partly coated with the evaported metal film M_2 as a base electrode. The glass plate was a 50 mm long, 40 mm wide and 0.15 mm thick glass slide. The xylene solvent was then volatilized gently at room temperature for a day. A thin PE film was thus formed and its thickness d ranged from 0.7 to 1.4μm depending on the polymer concentration in the solution. The heat treated samples had been prepared by heating at 140℃ for an hour and slowly cooling at a rate of about 0.1℃/min.

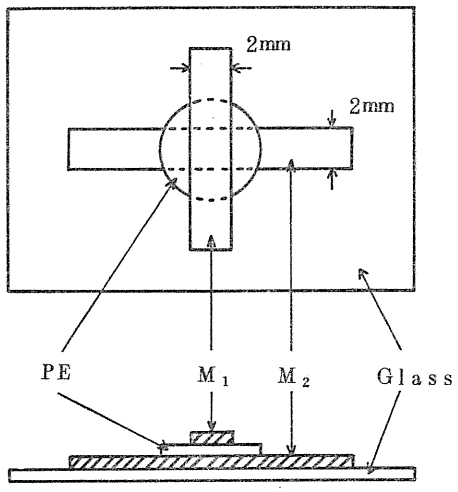

Fig. 9. Sample configuration: M_1 and M_2 indicate the top and base electrodes, respectively.

For the breakdown measurements, the metal M_1 was evaporated as a top electrode on the upper surface of the PE film. The final configuration of the sample was a capacitor of the M_1(top)-PE-M_2(base) tipe with a 2 mm×2 mm effective area as shown in Fig. 9. Most measurements were made on the Al-PE-Al system. The thickness of the metal electrode was monitored by the existance of the film which was deposited on a separate substrate set near the sample during evaporation, ranging from about 200 to 400Å. In most samples, the base electrode was thicker than the top electrode in order to be favorable for self-healing.[62, 63]

A ramp voltage of various rising speeds of 10^2, 10^4 and 10^6V/sec was applied to the sample in such a way that the base electrode was negative, such a condition being favorable for the self-healing.[62] Immediately after a breakdown occurred, the voltage was recorded with a peak voltmeter, and the breakdown test was repeated. The thickness of the PE film used for calculating the electric strength was estimated from the sample capacitance, assuming a value of 2.2 for the relative permittivity.

(ii) *Results and Discussion*

(a) *Morphology of PE Films*

An optical and electron microscopic study of the film surface revealed a significant difference in microstructure between the untreated and heat treated samples. An optical microphotograph of the untreated sample was featureless as shown in Fig. 10 (a), while a randomly oriented lamellae-like structure manifested itself on the same sample by a scanning electron microscope as shown in Fig. 10 (b). On the contrary, the heat treated sample exhibited spherulites accompanied by well-defined boundaries on the optical microphotograph as shown in Fig. 10 (c). Figure 10 (d) is the scanning electron microphotograph of the heat treated sample and is in accordance with the suggestion by Low et al.[64] that the spherulites are composed of ribbon-like lamellae radiating from a central nucleus and lamellae twist periodically about the radial direction.

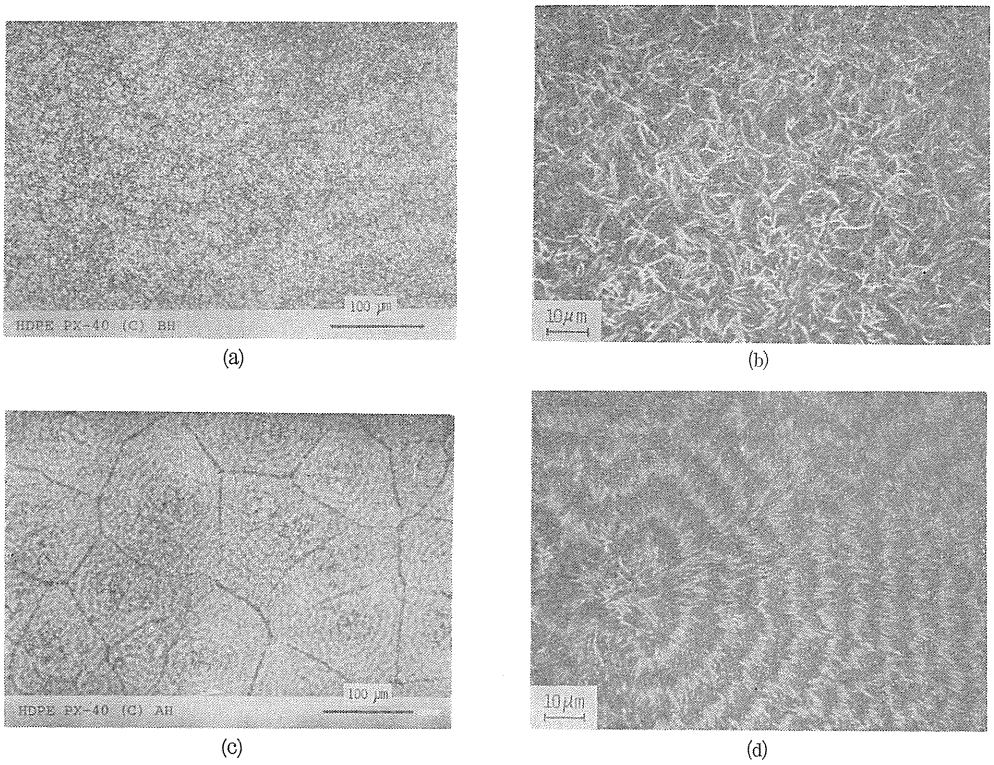

(a) (b)

(c) (d)

Fig. 10. Microphotographs of the surface of the PE films: (a) (b) the untreated samples and (c) (d) the heat treated samples; (a) and (c) are optical microphotographs, and (b) and (d) are electron scanning microphotographs.

(b) *Breakdown Characteristics*

Self-healing breakdown tests were done at room temperature on the thin film of PE with heat treatment. The number attached to the breakdown hole in Fig. 11 corresponds to the test number in Fig. 12 which gives F_B for each test number in order. A close look at the photo reveals that only one site corresponds to one applied ramp voltage with a few exceptions. The breakdown patterns can be classified into two types, single hole and propagating breakdowns. The latter has no relation to the intrinsic nature of the film. For the single hole breakdown, the breakdown occurs much more often at the spherulite boundaries, paticularly at the triple point of boundary lines, than at the inside of the spherulite. Effective thickness of the boundary is almost the same as that of the spherulite part. From these results, it will be concluded that the breakdown strength is lower along the spherulite boundaries, which is consistent with the direction of the preferred propagating path of tree breakdown in semicrystalline polymers. This implies that the role of the amorphous part for electrical breakdown differs between the spherulite boundary region and the interlamella region inside the spherulite, and the breakdown characteristics might be different between the directions, that is, whether it proceeds along the spherulite boundaries or across the series combina-

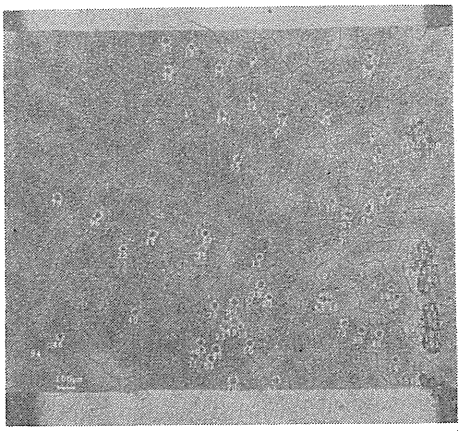

Fig. 11. An example of microphotograph on the 0.78μm thick sample after 100 tests: the number attached to each hole corresponds to the test number.

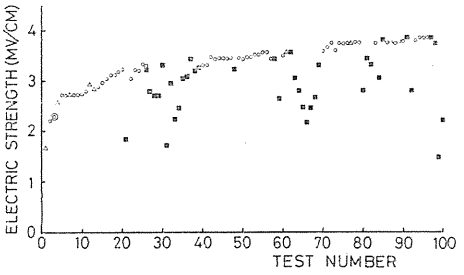

Fig. 12. F_B as a function of the test number of the same sample as for Fig. 11: closed squares indicate the propagating breakdown; and unfilled circles and triangles show the single hole breakdowns at the spherulite boundaries and at the inside of spherulite, respectively.

tion of the amorphous and crystalline regions.

Self-healing breakdown test was also made on PE thin films without heat treatment. As shown in Fig. 10 (a) and (b), the non heat-treated film has no spherulite and consists of randomly oriented lamellae, in contrast to the heat-treated film consisting of two-dimensional spherulites. F_B is shown as a function of votage rising speed dV/dt in Fig. 13. In this figure, the results for the heat-treated sample, in which the breakdown occurs mainly at spherulite boundaries, are also shown. Each point indicates a mean value for 10 succeeding self-healing tests on each specimen after weak spots were almost removed by applying a ramp voltage about

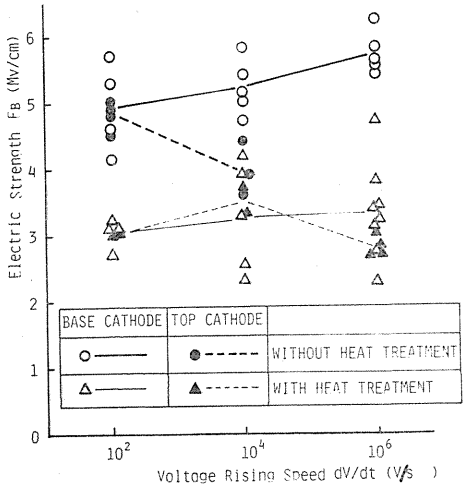

Fig. 13. F_B as a function of voltage rising speed for solution-grown PE thin films with and without heat treatment: The meaning of symbols are gives in inset; Each point gives a mean value for 10 sequential self-healing tests on a single specimen; and each line is drawn through an average of the points which represent the mean values on separate samples.

a hundred times, repeatedly. Each line is drawn through an average of above mentioned mean values for separate specimens under the corresponding condition which is indicated in inset of the figure. The polarity of applied voltage is designated 'top cathode' if the top electrode is a cathode, and the opposite polarity is denoted 'base cathode'. The features on the dependence of F_B on voltage polarity and voltage rising speed are similar to those for the heat-treated sample, and can be summarized as follows: (a) At dV/dt of 10^6V/sec, F_B with the base cathode, is higher than that with the top catode but at 10^2V/sec the polarity effect almost disappears. (b) With the base cathode, F_B at 10^2V/sec is lower than that at 10^6V/sec. Another experiments showed that F_B at -88℃ was slightly smaller than that at room temperature and F_B fell as the PE thickness increases at room temperature. These results indicates that the breakdown is related to an electron avalanche process.

(c) *Model for Breakdown Mechanism*

All the present results can be interpreted in terms of top surface roughness and electron space charge caused by injection, as follows. Supposing that the top surface is microscopically rough, at a high value of dV/dt, a high local electric field at a projection on the top cathode would not be relaxed because of few space charge, resulting in that the top cathode gives a lower value of F_B than the base cathode. With decreasing dV/dt, a space charge near the projection becomes sufficient to overcome the local electric field, and F_B increases toward the value for base cathode. The gradual decrease in F_B for the base catode with decreasing dV/dt is likely caused by an enhancement of electric field between the space charge front and the anode. This effect should be prominent for thin dielectric film like those in the present case

According to the above interpretation, F_B obtained at dV/dt of 10^6V/sec with the base cathode should be most close to a fundamental value free from both space charge and surface irregularity, and is about 5 MV/cm. This value is very close to ones published for conventional PE films whose thickness is usually beyond 10μm.[13, 37, 45]

Finally, a comparison between the heat-treated and non heat-treated samples is made. To avoid the influence of surface roughness, we will discuss the data with the base cathode. It can be recognized from Fig. 13 that F_B with the heat-treated sample is always lower within the present experimental limit of dV/dt than that with the non heat-treated sample. This fact indicates that the electric strength along boundaries between spherulites is lower than that in mixtures of randomly oriented lamellae and amorphous chains.

The remaining problem is to specify the breakdown characteristics in the region within a spherulite. In order to solve it. an improvement of the boundaries is necessary because the breakdown at the boundaries occurs before those can be obtained. Reinforcement of F_B is attempted by doping or oxidizing selectively to spherulite-boundaries. Such an approach would greatly contribute to a further improvement of polymer insulation system, and will be given in the following subsection.

(3) *Additive and Oxidation*

Some another heat-treated films were also prepared which had previously been doped with pyrene or dimyristyl-thio-dipropionate (DMTP)as a typical antioxidant.

Also, some heat-treated films were oxidized with an ozonizer.

Figure 14 shows the effect of doping and oxidation on F_B for the heat-treated films. Though the size of spherulites was decreased with doping of pyrene or DMTP because these impurities acted as a nucleus for crystallization, but two-dimensional spherulites could be formed. Doping of pyrene and DMTP at about 0.2 wt.% raised F_B and little change was observed with doping level while the heavy doping brought about a decrease in F_B. Almost the same result on the effect of doping additive on the electrical breakdown of PE was reported by Kolesov.[47] Probability for breakdown through the spherulite rose with doping. An increase in F_B and a decrease in probability of breakdown in spherulite boundaries with doping indicate reinforcement of the electrically weak spherulite boundary region by doping.

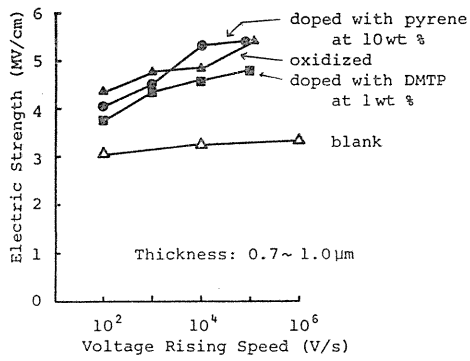

Fig. 14. Effect of dopeing and oxidation on F_B for the heat-treated PE films; each point is an agerage of 10 sequential self-healing tests on several separate samples.

Oxidation of the heat-treated films also increased both F_B and propability of breakdown through the spherulites as shown in Fig. 14. Since the oxidation was performed after two-dimensional spherulites were formed, no change in size of spherulite was observed and the oxidation might occur selectively to the spherulite boundaries because of quick diffusion of ozones.

2. 1. 3. High Temperature Region (Region Ⅲ)

In Region Ⅲ, the critical teperature T_{c2} (see Fig. 3) for HDPE is reported to be higher than that for LDPE.[4, 13, 37] The electric strength F_B increases with cross-linking[13, 22, 57] due to an increase of the softening point. These results suggest that erectromechanical deformation due to Maxwell stress is related to the electrical breakdown. It was also suggested from the relation between pre-breakdown current and F_B that thermal breakdown process is dominant.[65] Electronic thermal breakdown process[66] or breakdown basing on free volume theory[67] are considered as a dominant breakdown process after eliminating the electromechanical deformation. In this section, the effects of additive[29, 68] and cross-linking[57] are mainly discussed.

(1) *Additive*

It is generally known that insulation breakdown in thick insulations such as high-voltage, plastic-insulated power cables occurs in tree-shaped patterns, which reputedly are induced by voids and foreign substances in dielectric materials or on the boundary between conductors and such materials. Efforts are being actively pursued to preclude such occurrences by use of the so-called "voltage stabilizer" additives. In this subsection, the effect of additive on F_B at high temperatures is discussed.

The base resin is LDPE, to which additive, the anti-static agent AS-1 i. e. a type of boundary-surface activating agent, is mixed to specimen. Undoped or blank

PE is also used for comparison. The AS-1 agent is reported to have a low bleeding tendency and a good blending property with PE.[69] Table 7 shows the physical properties of the base resin and additives.

Figures 15 shows the temperature dependence of F_B in the blank PE and the resin doped with the AS-1 (1 wt.%). At high temperatures above room temperature F_B of PE doped with AS-1 is lower than that of blank PE, and decreases with increasing temperature. The AS-1 specimen exhibits a lower value of F_B for applying dc than that for applying pulse. The conduction characteristics of PE doped with AS-1 and blank PE are shown in Fig. 16. It is found from all the results that additive (AS-1), which supplies a charge carrier and increases the electrical conductivity, lowers F_B at high temperature due to the thermal breakdown process.

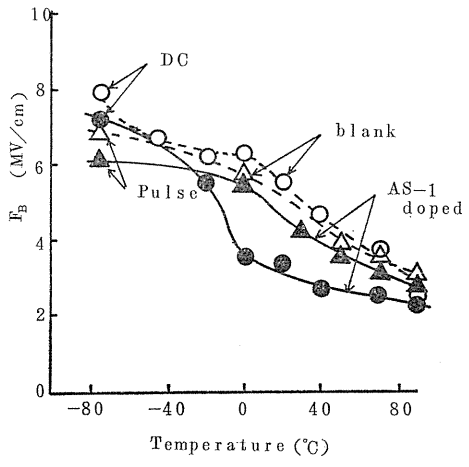

Fig. 15. Temperature dependence of F_B of PE with and without AS-1.

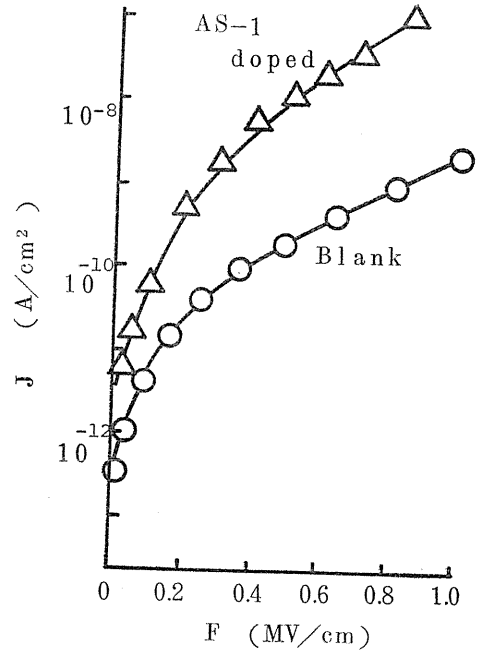

Fig. 16. High-field conduction of AS-1 doped PE.

(2) *Cross-linking*

Cross-linking is expected to cause an increase in F_B in the temperature region where the mechanical deformation is effective. In this subsection, the effect of cross-linking on the breakdown characteristics of PE is examined. Correlation of mechanical properties to F_B in the high temperature region to 160℃ is mainly discussed.

Specimens were two kinds of 25μm thick silane cross-linked PE (Linkron X. Mitsubishi Petrochemical Co. Ltd.) with different gel content which gives a measure of cross-linking. The physical parameters of these films are listed in Table 8, as well as that of PE-1 which is the base polymer of the cross-linked PE and

Table 8. Physical parameters of silane cross-linked PE.

	Density (g/cm^3)	M. F. R. (g/10min)	Silan content (weight %)	Gel content (weight %)
Si-1	0.921	1.2	0.5	73
Si-2	0.928	4.0	5.0	96
PE-1	0.917	1.0	—	—

contains no silane group.

Figure 17 shows the temperature dependence of F_B for the silane cross-linked PE by applying a ramp voltage at the rate of 500V/sec. This figure also contains the result of PE-1. It can be seen that in a temperature region from room temperature to about 90℃, F_B for Si-1 is almost the same as that for PE-1 and decreases with increasing temperature Above 90℃, a variation in F_B for Si-1 is small. On the other hand, F_B for Si-2, which has a higher degree of cross-linking, is equal to that for PE-1 from room temperature to 50℃, while from 50℃ to 160℃, is higher than those for either PE-1 or Si-1. The effect of cross-linking due to high energy radiation on F_B of PE at high temperature has been studied.[13, 22] The cross-linking leads to the rise of the softening point and resulting in a marked increase in F_B. A similar behavior is also obtained for the case of the silane cross-linking PE.

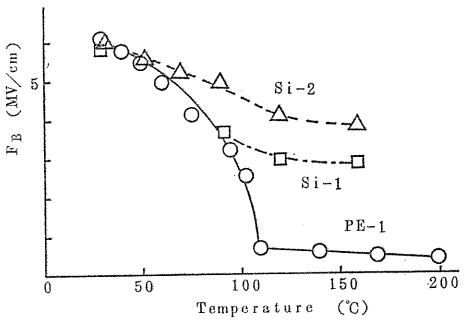

Fig. 17. Temperature dependence of F_B by applying a ramp voltage at the rate of 500 V/sec for PE with a different degree of cross-linking.

The measurements of Young's modulus were also made with the cross-linked PE.[57] It was found that F_B above room temperature could be expressed as a function of Young's modulus, irrespective of the sample type or temperature. However, no good agreement between the theoretical strength and the experimental one was obtained. although the dc breakdown characteristics of PE and silance cross-linked PE were found to be closely related to Young's modulus.

2. 2. Electrical Breakdown of High Temperature Polymers

2. 2. 1. Introduction

The rapid development of synthetic chemical engineering in recent years has brought new type polymeric electrical insulating materials to endure under extreme conditions of temperature, radiation, chemical environment etc. Among them, polyimide (PI) and polyamideimide (PAI) have been expected as superior electrical insulating materials to be applied at very high temperatures because of their excellent thermal properties.[70, 71] However, very few investigations[72~75] have been reported on their electrical breakdown characteristics The purpose of this section is to elucidate the electrical breakdown mechanism of PI and PAI films especially

in high temperature region. Being founded on this conclusion about the breakdown mechanism, the heat and hydrolytic treatment effects on their electrical breakdown were also studied.

2. 2. 2. *Experimental Procedure*

Measurements were made on PI films (KAPTON-H) of about 26, 52 and 78μm in thickness and PAI films (PAIFRON-2) of about 25 and 50μm. Samples were sandwiched with the sphere-plane electrodes and were immersed in silicone oil or lig. N_2 at a constant temperature. After the sample was immersed for about 5 minutes, a linearly rising dc voltage was applied at various rising rates.

2. 2. 3. *Results and Discussion*

(1) *Electrical Breakdown of Polyimide Film*

The temperature dependence of F_B of as-received PI film is shown in Fig. 18 with open circles. It can be seen that in low temperature region below room temperature (region I), F_B scarcely varies with temperature, suggesting an electronic breakdown process.[3] On the contrary, in high temperature region above room temperature, F_B decreases with rising temperature (regions II and III) and falls steeply especially above 200℃ (region III). There are three possible mechanism by which the negative temperature coefficient of F_B can be explained.[3] Among them the thermal breakdown can be considered as the most possible mechanism in regions II and III: The theoretical value of F_B in the electromechanical breakdown can be estimated at about 200 MV/cm and this value cannot be compared with the measured values of 0.9~4.9 MV/cm; and Fröhlich's amorphous theory cannot explain the result that F_B depends on the rising rate of electric field in regions II and III as shown in Fig. 19.

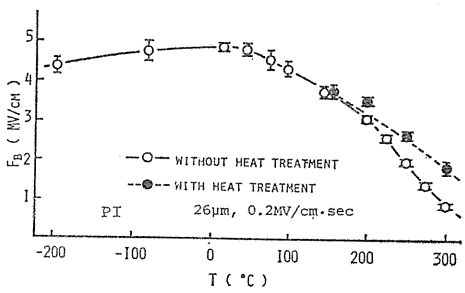

Fig. 18. Temperature dependence of F_B of polyimide film (heat treatment; about 300℃, 7 days).

In general, the fundamental equation for thermal breakdown is given as

$$C_v(dT/dt) - \mathrm{div}(\kappa \mathrm{grad} T) = \sigma F^2 \tag{3}$$

where C_v is the specific heat per unit volume, κ and σ are the thermal and the electrical conductivities, respectively. In the case of impulse thermal breakdown, the heat conduction term in eq. (3) disappears, resulting in

$$C_v(dT/dt) = \sigma F^2. \tag{4}$$

The impulse thermal critical field strength obtained by solving eq. (4) depends on the rising rate of electric field α but not on the sample thickness (d).[3] As shown in Figs. 19 and 20, the present experimental results in region III are consistent with this expectation. In region II, however, F_B depends on d as well as α. This suggests that in region I the thermal conduction of the sample also plalys a role in contrast to region III. In summary, as temperature rises, the second term in

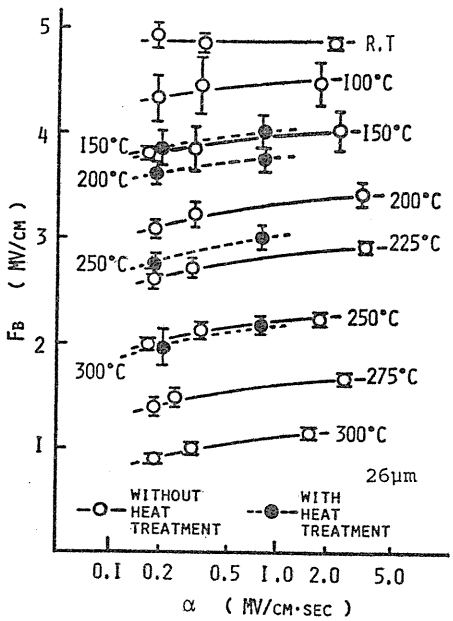

Fig. 19. Dependence of F_B of PI film on rising rate of electric field (heat treatment: about 300℃, 7 days).

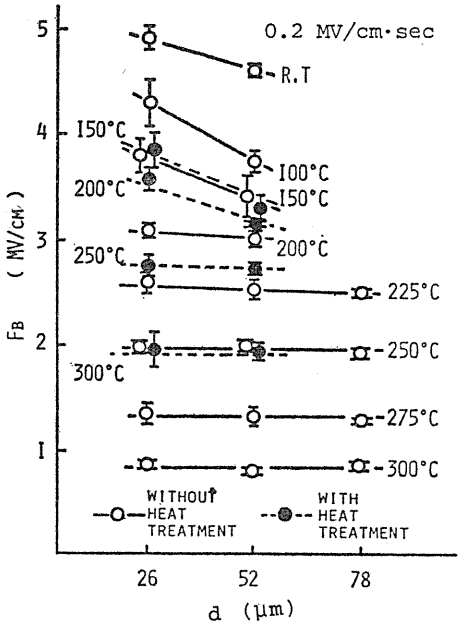

Fig. 20. Dependence of F_B of PI film on sample thickness (heat treatment: about 300℃, 7 days).

the left hand side of eq. (3) tends to be neglected as compared with the first term. As a possible reason for this, two interpretations can be given as follows: (1) the heat conduction from the sample is reduced due to the rise of temperature in the surrounding medium; and (2) the increase in the electrical conductivity with temperature leads to the rise of energy input per unit time which reduces a role of the heat conduction in the breakdown and this leads to the impulse thermal process as the temperature rises.[34] The critical temperature between regions Ⅱ and Ⅲ is estimated at about 200℃ for α of about 0.2 MV/cm·sec, but this value is considered to vary with α and σ of the sample.

When the thermal breakdown is operative, the electrical conduction of the sample greatly influences its electrical breakdown. Regarding the electrical conduction of PI film at high temperatures, Sacher[76] suggested that the charge carrier is protonic and supplied from the residual non-reacted polyamic acid left in as-received PI films. Therefore, the heat treatment of the as-received PI film in an air oven at about 300℃ was made in order to convert the residual polyamic acid to PI. As shown in Figs. 21 and 22, above 200℃, σ decreases and F_B increases with the heat treatment, but below 200℃ σ and F_B are almost independent of the heat treatment. These relations between σ and F_B are consistent with the thermal breakdown. The breakdown characteristics of the heat treated samples are shown in Figs. 18, 19, and 20 with closed circles. At 150℃ F_B scarcely varies with the heat treatment, but above 200℃ the breakdown characteristics of the heat treated samples are similar to those of the as-received samples measured at the lower temperature and especially the thickness dependence of F_B at 200℃ appears with

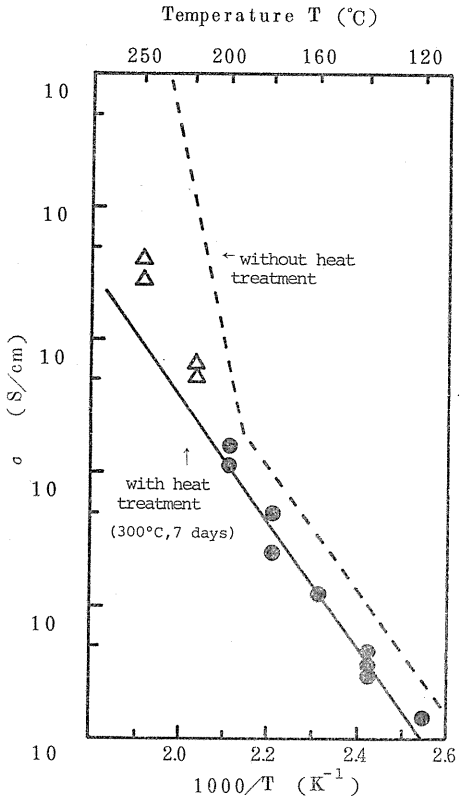

Fig. 21. Influence of a high temperature-long period heat treatment on the temperature dependence of electrical conductivity.

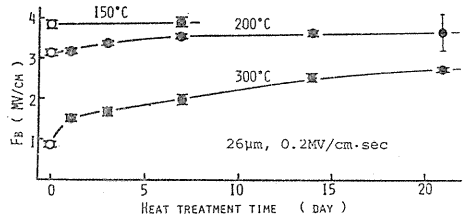

Fig. 22. Heat treatment effect on F_B of PI film (heat treatment: about 300℃).

the heat treatment. These results show that the critical temperature between regions Ⅱ and Ⅲ shifts to the higher temperature with heat treatment, being interpreted in terms of the decrease of σ with heat treatment.

In order to elucidate further the relation between polyamic acid in PI and the electrical breakdown, the effect of hydrolytic and succeeding heat treatments on F_B was studied, where the hydrolytic treatment was done at room temperature by the following process: As-received PE film was immersed in about 2N KOH solution for 18 hours, and dried in vacuum for a day. Then, the sample was immersed in about 1N HCl solution for 9 hours, washed by water to remove the adhering HCl, and dried in vacuum for two weeks. As shown in Fig. 23, F_B decreases with the hydrolytic treatment at first and increases gradually toward that of the as-received sample with the succeeding heat treatment in silicone oil at 200℃. The change of the amide bands around 1682~1670cm^{-1} and 1550cm^{-1}, and the imide bands around 1780cm^{-1}, 1360 cm^{-1} and 720cm^{-1} in the infra-red spectrum showed that the amount of polyamic

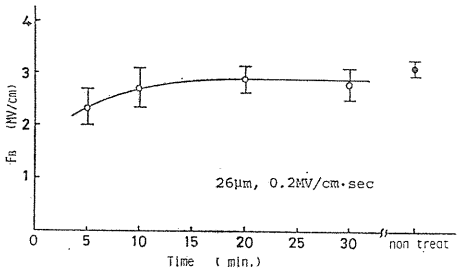

Fig. 23. Effect of heat treatment on F_B of hydrolyzed PI film (heat treatment: 200℃ in silicone oil).

acid in the PI film increased with the hydrolysis, but gradually decreased with the heat treatment.[78,79] These results are consistent with the breakdown result of the as-received samples as mentioned above.

(2) *Electrical Breakdown of Polyamideimide Film*

The dependence of F_B of as-received PAI film on temperature is shown in Fig. 24 with open circles. In high temperature region F_B decreases with increasing temperature. It was also found that F_B depended on α and was independent of the sample thickness. From these results, the electrical breakdown mechanism of PAI film above room temperature is considered to be thermal breakdown with a similar consideration to that of PI film. The heat treatment effect for F_B of PAI

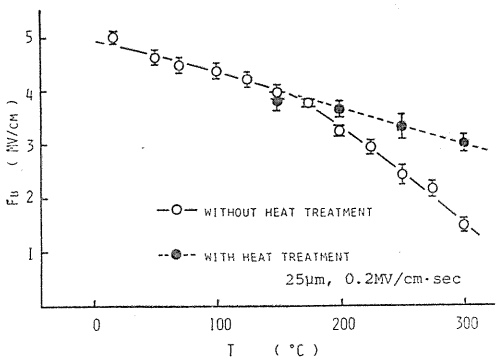

Fig. 24. Temperature dependence of F_B of polyamideimide film (heat treatment: about 310℃, 5 hours).

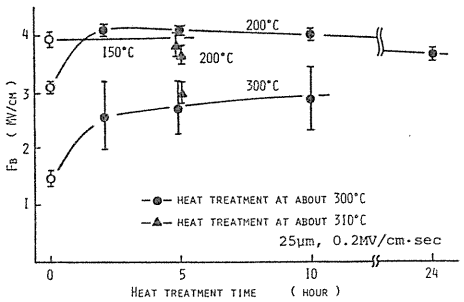

Fig. 25. Heat treatment effect on F_B of PAI film.

film, which is shown in Fig. 25, is also similar to that of PI film. In the case of PAI film, however, the heat treatment effect becomes effective in a shorter time than in PI film, and at 200℃ there appears a decreasing part of F_B with increasing the heat treatment time after F_B shows a maximum value, suggesting the relation to the poor thermal resistance as compared with PI film.[70,71]

2. 3. Electrical Breakdown of Poly (vinylidene-fluoride)

2. 3. 1. Introduction

The advancement of the chemical engineering of synthetic materials has introduced many new polymers, some of which play an important role in the field of electrical and electronic engineering. Among them, poly (vinylidene-fluoride) (PVDF) is expected to have practical applications, making use of its piezoelectricity and pyroelectricity.[80] Recently PVDF was also proposed as a dielectric material for a high energy density capacitor because of its high dielectric constant as compared with the other polymerised materials.[81]

PVDF is a polar and highly crystallized polymer, with chemical structure of $(-CH_2-CF_2-)_n$. It has two representative stable crystalline phases; α-phase and β-phase.[82] The β-phase can be formed by uniaxial stretching, and electrets manufactured from the film involving β-phase show strong piezoelectricity.[83] The β-phase has a planer zigzag type conformation with a large dipole moment of CF perpendicular to the main chain. Its lattice constants are reported to be as

follows: a=8.58 Å, b=4.91 Å, and c=2.56 Å. On the other hand, in the α-phase with helical conformation, dipoles are cancelled out in unit cell, and its lattice constants are: a=4.96 Å, b=9.64 Å, and c=4.62 Å.

The dielectric properties have been extensively studied by many authors.[84] However, much remains unknown about the electrical insulaing properties which are necessary for its application. Especially, the electrical breakdown of PVDF has been insufficiently clarified.

In this section, the electrical breakdown of PVDF with different types of crystalline structure is studied over the temperature range from room temperature to 150℃. The breakdown mechanism is discussed in detail in the high temperature region above 50℃. In addition, the theoretical impulse thermal breakdown strength is calculated assuming ionic conduction. On the basis of the computation, an estimation of the conduction parameters is made from fitting the theoretical values of breakdown strength to the experimental charecteristics.[30, 31, 85] From these experimental results, the relation between the solid structure and electrical breakdown of PVDF is also discussed.[31]

2. 3. 2. Experimental Procedure

Specimens of PVDF with almost the same degree of crystallinity but different ratio of α-phase to β-phase were used for breakdown measurements. Physical properties of these specimen are given in Table 9. The ratio of the two types of crystalline phases was determined from D_α/D_β which is the ratio of the absorption at 530cm^{-1} at which the specific peak for α-phase in the low frequency region appears, to that at 510cm^{-1} which is the specifik peak for β-phase (D is the magnitude of absorption).

Table 9. Physical parameters of the specimen.

Sample type	Infrared absorption ratio D_α/D_β	Thickness (μm)
Unstretched	—	35
Biaxially stretched	1.5	12
Uniaxially stretched A	1.1	15
Uniaxially stretched B	$<$0.05	15

2. 3. 3. Results and Discussion

The temperature dependence of electric strength F_B for various types of films was obtained at a field rising rate of 0.2MV/cm·sec in the temperature range from room temperature to 150℃. The result is shown in Fig. 26. It was found that F_B for biaxially stretched film above 50℃ was independent of the sample thickness between 25 and 50μm. The thickness of the present samples was different for different types of PVDF films as shown in Table 9. Nevertheless, if the assumption is made that F_B is independent of the sample thickness in all cases, it is inferred from Fig. 26 that as the proportion of α-phase increases, F_B is lowered, except for an unaxially stretched film B in the temperature range above 100℃. For the unaxially stretched film B, F_B steeply decreases above 100℃. This is possibly due to the relaxation of larger residual internal strain compared to the

other films since this film was made by low temperature stretching. Therfore, the data beyond 100℃ for the uniaxially stretched films B are precluded from the following analysis.

Next, F_B for various types of films was obtained at 100℃ by varying field rising rate from 0.03 to 0.8MV/cm·sec. These results are shown in Fig. 27. It is

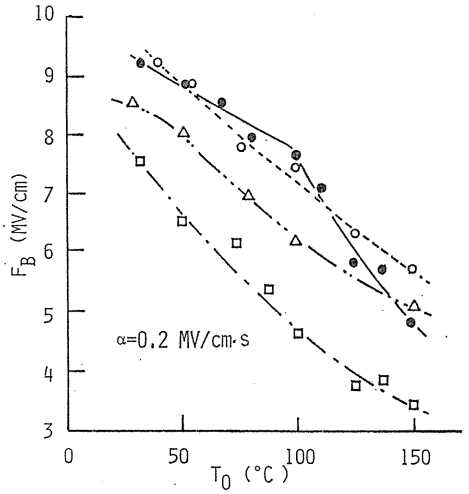

Fig. 26. Temperature dependence of F_B for various types of PVDF. Rate of increase of electric field $\alpha=0.2$ MV/cm·sec. □-unstretched film, △-biaxially stretched, ○-uniaxially stretched film A, and ●-uniaxiallity stretched film B.

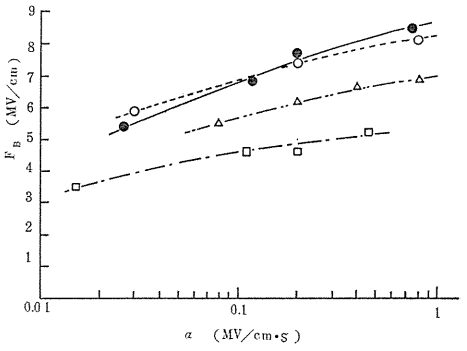

Fig. 27. Relation between F_B and rate of increase of field at 100℃. Symbols as in Fig. 26.

seen that in in each type of film, F_B increases with increasing field rising rate. From this fact as well as the negative temperature dependence of F_B, the thermal breakdown is considered to be operative for all types of films above room temperature by following the same arguments as for polyimide film as given in Section 2. 2. Therefore, assuming the impulse thermal breakdown as a possible breakdown mechanism, the analysis of the result was made using the numerical calculation to estimate ionic conduction parameters for each sample. Here, we will show the procedure of numerical analysis briefly. The equation of the impulse thermal breakdown is

$$C_v(\mathrm{d}T/\mathrm{d}t)=jF, \tag{5}$$

where meanings of the symbols are already given in Section 2. 2. The ionic current density j can be expressed as

$$j=j_0\exp(-\phi/kT)\sinh(qa_iF/2kT) \tag{6}$$

where, j_0 is a constant, ϕ is the zero-field activation energy, q is the ionic charge, a_i is the ionic jump distance, k is Boltzmann's constant. Using the relation $F=\alpha t$

(α: field rising rate) and changing a variable from t to F, equation (5) becomes a first order ordinary differential equation with respect to dependent variable F. The temperature as a function of F was computed. In this calculation, the critical temperature T_m required for breakdown was taken as 180℃, the melting point of PVDF, for convenience, and the electric field at which the specimen temperature reaches T_m was regarded as the theoretical electric strength.

The conduction parameters for each type of specimen can be evaluated by fitting the theoretical results to the experimental ones.[30] Figures 28 and 29 shows the typical results for the unstretched film on the theoretical dependence

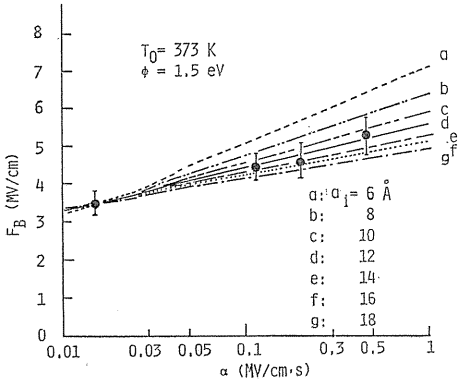

Fig. 28. Theoretical relation between F_B and α for different values of a_i for the unstretched film. Ambient temperature T_0=100℃, ϕ=1.5eV, and j_0 is varied so that F_B at α=0.0015MV/cm·sec for each value of a_i coincides with experimental breakdown data; ●-experimental values.

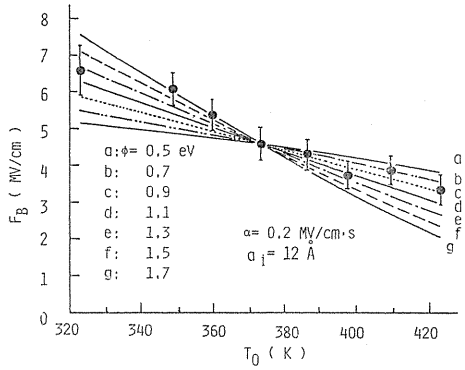

Fig. 29. Theoretical dependence of F_B on the ambient temperature T_0 for different values of ϕ for the unstretched film: α=0.2MV/cm·sec, a_i=12 Å, and j_0 is varied so that F_B at 100℃ for each value of ϕ coincides with experimental breakdown data; ●-experimental values.

of F_B on temperature and on field rising rate, respectively. Here, the experimental data are indicated by filled circles. It can be seen from both figure 28 and 29 that the best fit of the experimental plot to the theoretical curve is attained when a=1.2 Å, ϕ=1.1 eV and j_0=9.3×10^{9}A/m^2 for the unstretched film. The same analysis was carried out for the breakdown results of uniaxially stretched

Table 10. Ionic conduction parameters obtained from fitting theoretical electric strength to the experimental ones.

Parameter	Unstretched	Biaxially stretched	Uniaxially stretched A	Uniaxially stretched B
Ionic jump distance (Å)	1.2	9	9	6
Activation energy (eV)	1.1	0.9	0.9	0.5
Pre-exponential factor (A/m^2)	9.3×10^9	1.2×10^7	1.8×10^6	2.5×10^2

films A and B and biaxially stretched film. The ionic conduction parameters thus obtained are summarized in Table 10. It is found that both the jump distance and the activation energy, apparently increase with increasing the proportion of α-phase and thus decreasing the proportion of β-phase involved in the sample. It is concluded, therefore, that the change in the crystalline structure for PVDF would be associated with the change in the ionic conduction parameters as estimated from the breakdown data. However, at present, the physical meaning of these results is still not well understood, so that further investigation must be attempted.

2. 4. Electrical Breakdown of Plasma Polymerized Styrene Thin Films

2. 4. 1. Introduction

Plasma polymerized thin films which are made through polymerization of organic vapors in a glow discharge have many advantages; for example, a small number of pinholes and a high temperature resistance resulting from the highly cross-linked structure compared with those of conventional polymers. In addition, this polymerization method is so easy that they are expected to have practical applications to thin film capacitors, field effect transistors,[86] switching elements [87, 88] and so on.

Thin films have a great advantage by making use of self-healing[62] in the study of electrical breakdown, since localized weak spots can be eliminated and a large number of breakdown experiments can be made on one sample. In this section the electrical breakdown of plasma polymerized styrene thin films, which is denoted by PPS, is studied by taking advantage of self-healing. We then discuss the electrical breakdown mechanism from these experimental results.[89~91]

2. 4. 2, Experimental Procedure

PPS was grown in a glow discharge at a styrene monomer pressure of 0.5 Torr, a current density of about 1 mA/cm^2 and a frequency of 5 kHz. This film was sandwiched between the top and base elecrodes fabricated on a glass substrate (Fig. 30). The polymer thickness was estimated from the capacitance, assuming 3 for the dielectric constant,[62] and ranged from 2000 to 4500 Å.

Prior to all the experiments, several hundred self-healing breakdown were performed untill breakdown voltages reached a nearly constant value in dry nitrogen gas at a pressure of 1 atm. at room temperature by applying a single ramp voltage at a voltage rising rate dV/dt of 250kV/sec. Some measurements were made on time lag applying a step voltage. The effect of dc prestress was also studied. Positive or negative prestress F_p in a range up to 3 MV/cm was applied for a given period t_p immediately before a positive ramp voltage at 250 kV/sec was imposed on the sample.

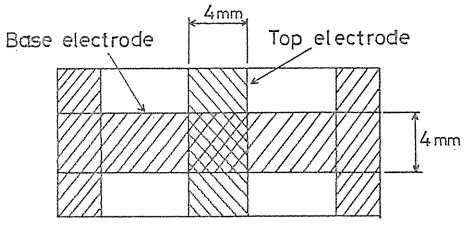

Fig. 30. Shematic diagram of sample.

2. 4. 3. Experimental Results

A typical result of the temperature dependence of electric strength F_B of

Au-PPS-Au at 250kV/sec is shown by full circles in Fig. 31. It is seen from the figure that F_B scarcely changes with temperature over 0 to 200℃.

Figure 32 shows the relation between F_B and the field rising rate α for Au-PPS-Au at room temperature. It is seen that F_B strongly depends on α over a wide range from 10^7 to 10^{13}V/m·sec.

Some measurements were made on the effect of electrode metal on F_B by using both sample structures of Au-PPS-Al and Al-PPS-Au. In both types, F_B

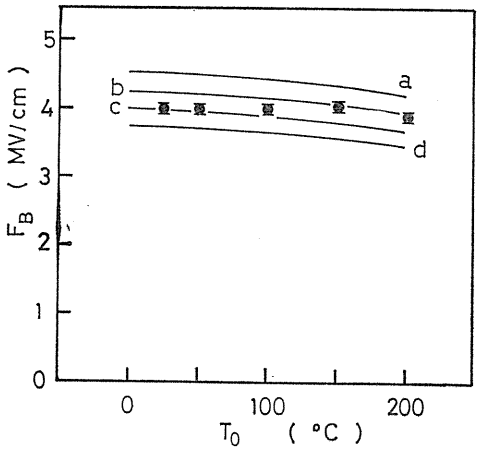

Fig. 31. Temperature dependence of F_B for Au-PPS (2300 Å)-Au: filled circles indicate experimental values; and solid lines indicate theoretical ones with a parameter of contact barrier hieght Φ_D: (a) 1.05, (b) 1.0, (c) 0.95, (d) 0.9.

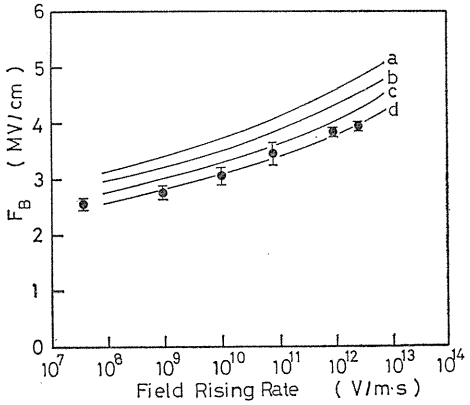

Fig. 32. Relation between F_B and α for Au-PPS (2600 Å)-Au. Meanings of symbols are the same as for Fig. 31.

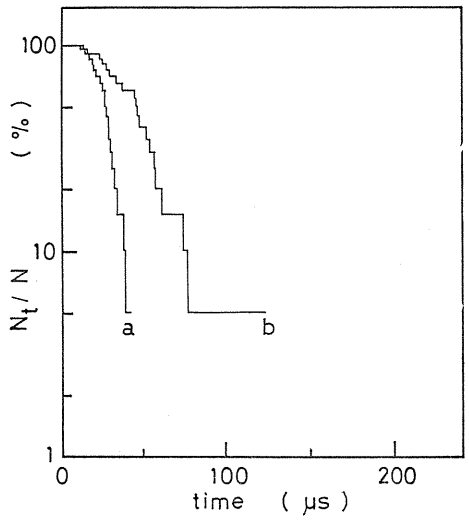

Fig. 33. Effect of electrode metal on time lag on applying step voltage of 5.0 MV/cm for Al-PPS (3200A)-Au. (a) Au as anode and Al as cathode, and (b) Au as cathode and Al as anode.

for the Au cathde was slightly higher than that for the Al cathode. This effect appeared only slightly in F_B, but manifested itself in time lag evaluated from so called Laue plots[14] as shown in Fig. 33. It is found that the Au catode gives a longer time lag than the Al cathode. It is also found that the formative time lag was about 10^{-4} to 10^{-5}sec, which is unusually long.

In addition we measured F_B of Au-PPS-Au in various kinds of ambient gases at room temperature. Oxygen atmosphere gave a higher value of F_B by about ten percent than both vacuum and nitrogen atmospheres in which F_B was almost identical. It was also found that for Au-PPS-Au the time lag in O_2 was longer than that in N_2, being consistent with the above mentioned ambient effect on F_B.

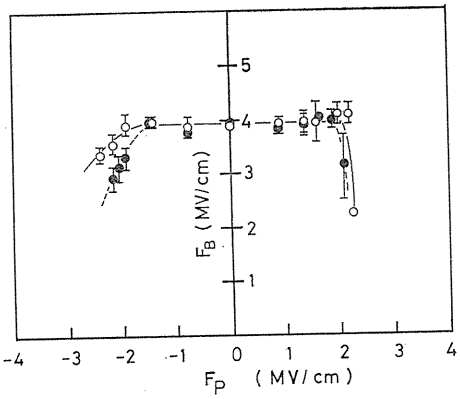

Fig. 34. Effect of prestress on F_B at 23℃ for different prestress times for Au-PPS (2600 Å)-Au. Unfilled and filled circles indicate F_B for 60 and 180sec prestress time, respectively.

F_B decreases with increasing prestress as shown in Fig, 34. The shape of the curve F_B vs. prestress was almost independent of either the polarity of prestress or the temperature over −196 to 100℃.

2. 4. 4. Discussion

We will discuss the breakdown mechanism of PPS on the basis of the above results, which can be summarized in Table 11.

Table 11. Breakdown characteristics of PPS.

temperature dependence	$\partial F_B/\partial T_0 \simeq 0$ (0 to 200℃)
field rising rate dependence	$\partial F_B/\partial \alpha > 0$
electrode metal effect	F_B(Au cathode) $\geqq F_B$(Al cathode)
ambient atmosphere effect	F_B(in O_2) $\geqq F_B$(in N_2, vacuum)
prestress effect	F_B decreases with both porarities of prestsess field

F_B: electric strength, T_0: ambient temperature, α: field rising rate.

First of all, the cathode metal and ambient atmosphere effects indicate that electrons injected from the cathode play an important role in the breakdown process; the effective barrier height Φ_D for Au-polymer contact would be higher than for Al-polymer one; and O_2 gas adhering on the metal-insulator interface would form surface states, leading to an increase in Φ_D.[92] Secondly, taking into account the little variation of F_B with temperature, a temperature independent injection process is considered to be dominant. Thirdly, F_B strongly depended on α and was lowered by both polarities of prestress field. The time lag to breakdown obsereved was of the order of 10^{-4} to 10^{-5}sec, considerably longer than that usually expected for a pure electronic process.[20] These facts are thought to

support the concept of thermal breakdown.

On the basis of the above consideration we will present a new simple model of breakdown: The current is controlled by a tunnelling emission from the cathode and the bulk breakdown is governed by the impulse thermal process. In this model it is assumed that space charge in the bulk and heat conduction towards the surroundings are neglected.

We start with the differential equation for the impulse thermal breakdown which is already given by eq. (5) in Section 2. 3. We introduce here as j in eq. (5) the Fowler-Nordheim tunnelling emission[93] given as

$$j=AF^2\exp(-B/F), \tag{7}$$

where

$$A=2.2e^3/8\pi h\Phi_D \tag{8}$$

and

$$B=8\pi(2m^*)^{1/2}\Phi_D{}^{3/2}/(2.92he), \tag{9}$$

where e is the electronic charge, h Planck's constant, m^* the effective electronic mass. When the electric field rises proportionally with time, i. e. $F=\alpha t$, eq. (5) can be transformed to

$$(\mathrm{d}T/\mathrm{d}F)=AF^3\exp(-B/F)/(C_v\alpha), \tag{10}$$

by using eq. (7). This ordinary differential equation can be solved numerically. In the following alculation, it is assumed that $C_v=2.0\times10^6$ J/K·m^3 and m^* is the mass of a free electron.

We shall estimate Φ_D by fitting the theoretical results to the experimental ones. The theoretical dependence of F_B on the ambient temperature T_0 was calculated for different values of Φ_D at α of 8.3×10^{13} V/m·sec, which is already given in Fig. 31 with the solid lines. It can be seen from the figure that the best fit of the theoretical curve to the breakdown data is attained when Φ_D is about 1 eV. The theoretical relation between F_B and α at 300K is shown for various values of Φ_D in Fig. 32. This calculated relationship agrees well with the experimental one, provided Φ_D is about 0.9 eV. The calculation of prestress on F_D was also carried out, and it was found that the results were in good agreement with the experiments when $\Phi_D=1.05$ eV.

From the above results it can be concluded that this simple model can give a quantitative explanation to the experimental data such as F_B-T_0, F_B-α and prestress effect on F_B, provided Φ_D is about 1 ev. The cathode metal and ambient atmosphere effects can be also interpreted qualitatively in terms of the variation of Φ_D.

In this simple model we have not been so far concerned with the bulk processes such as collision ionization and recombination etc. Here electronic collision ionization and hole removal by drift are, therefore, considered as a possible bulk conduction.[94] We will introduce the bulk process into our breakdown model.[91]

Figure 35 shows a typical example of the theoretical current density as a function of the electric field for different values of the mobility of holes μ_p. Using the current density and the field distribution, eq. (10) was solved numerically. The theoretical electric strength was determined by the preceding events

described defined by either the impulse thermal criterion or the negative resistance criterion. Obviously, the latter criterion could not explain the existence of the field rising rate and prestress effects, since it contains no time component. The calculated results based on the former criterion were almost in agreement with the simple model without taking the bulk process into consideration, provided μ_p is beyond a certain value. This gives a physical basis for neglecting the space charge in our model.

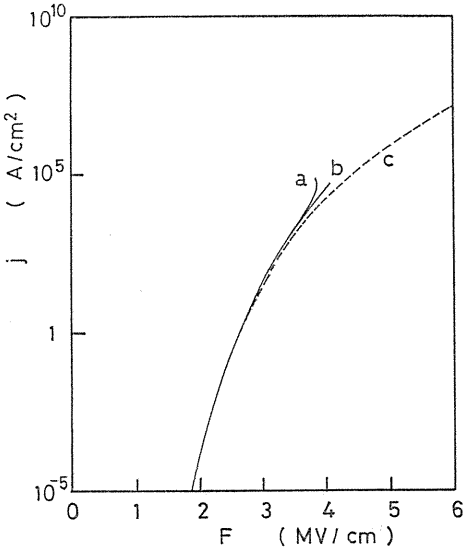

Fig. 35. Theoretical current-field characteristics for different hole mobilities μ_p: (a) $\mu_p=10^{-8}$m^2/V·sec, (b) $\mu_p=10^{-7}-10^{-4}$m^2/V·sec, and (c) a broken line represents Fowler-Nordheim tunnelling esimmsion current.

3. Electrical Treeing Breakdown

When the thickness of the insulation system is relatively thick, electrical treeing breakdown is one of main factors of the failure of the polymeric insulating material. It can be observed that these electrical trees develop from the conductor of the power cable to the insulating solid and arise from some sort of defects or voids within the material. Electrical treeing is recognized as a tree-shaped track remaining after a decomposition and vaporization of solid due to partial discharge or electron avalanches. However, the detail understanding of the electrical treeing breakdown is not fully given. In this chapter, we discuss the fundamental process of electrical treeing breakdown.

3. 1. DC Treeing Breakdown

3. 1. 1. Introduction

Recent development of dc power transmission has brought many problems concerning the electrical insulation of various related equipment operating under direct voltage and various associated voltage wave forms (polarity reversal, switching etc.). In addition, many uncertainties remain with regard to the dc testing of ac cables, such as its equivalency and the insulation degradation under dc stress.

Many investigations have been made of the stress distribution in dc insulation systems which is mainly based on the electric resistance as a function of temperature and dc stress. Little attention has been paid to the field distortion due to space charge accumlation (homo- and hetero-charges).[1, 95, 96]

In order to understand the effect of space charge on a dc insulation system, in this section, dc treeing phenomena initiated from the tip to a needle electrode inserted into a polyethylene specimen are investigated under various conditions,

and the mechanism of space charge formation is also discussed.

3. 1. 2. Experimental Procedure

Thick plates of low density polyethylene (LDPE, 25×25×5 mm) were used as shown in Fig. 36. A metal needle electrode having a radius of curvature of 5 μm was molded into each plate in such a way that the distance between the tip of the needle and the bottom surface of the plate, which was painted with silver paste, was either 2 or 5 mm. This electrode arrangement is often used in treeing breakdown tests, which simulated structural defects (impurity, internal defect, electrode irregularity) present in a prctical insulation system. The specimen is immersed in silicone oil at a controlled temperature or in liquid nitrogen.

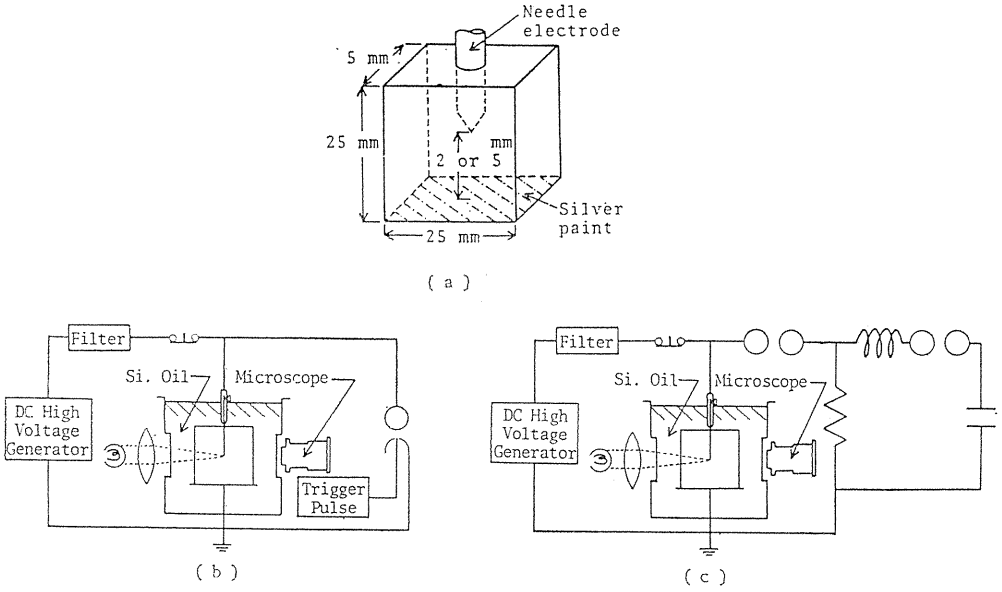

Fig. 36. Block diagrams of experimental circuits and specimen. (a) Electrode arrangement of specimen, (b) Short-circuit tree, and (c) Polarity reversal tree.

3. 1. 3. Results and Discussion

Under nonuniform divergent fields, a partial breakdown is usually observed at the site of the strong localized electric field.[96] A trace of this partial breakdown is called a "tree" from the characteristic feature of their breakdown paths. The tree initiated by a dc voltage application is strongly affected by space charge formation. We consider four kinds of tree initiation depending on the different voltage application procedure as follows.

(a) *DC voltage tree*: This tree is initiated from the tip of the needle on the application of linearly rising dc voltage.

(b) *Short-circuited Tree*: This tree is observed when both electrodes are short-circuited after the application of dc voltage which is lower than the dc tree inception voltage.

(c) *Polarity reversal tree*: This tree is observed when an impulse of opposite polarity is applied after dc voltage prestressing. The sample is left open-circuited for the time between the application of dc and impulse voltages.
(d) *Impulse tree*: This tree is initiated by the application of impulse voltage (1/40 μsec.)

(1) *Voltage Rising Rate and Tree Inception Voltage (dc voltage tree)*

The tree inception voltage V_i is defined here as the applied voltage when a tree of 10μm in length is observed under the microscope around the tip of the needle electrode with rising the dc voltage at a constant rate. As shown in Fig. 37, V_i, decreases with increasing voltage rising rate for both polarities and V_i for the negative polarity is greater than that for the positive one. The electric field at the needle tip calculated from V_i in Fig. 36 is much greater than the electric strength of polyethylene (PE). For example, V_i at the rising rate of 10^3V/sec gives 27MV/cm which is about 5 times as large as F_B of PE. It can be concluded from these results that homo space charge accumulated near the needle electrode during the dc voltage applcation, causing a field moderation near the neele tip. The dependence of V_i on the voltage rising rate is significant because it is directly related to the time for the accumulation of space charge. The polarity effect suggests that the characteristics of the homo space charge formed near the needle must be dependent upon the polarity of the applied voltage.

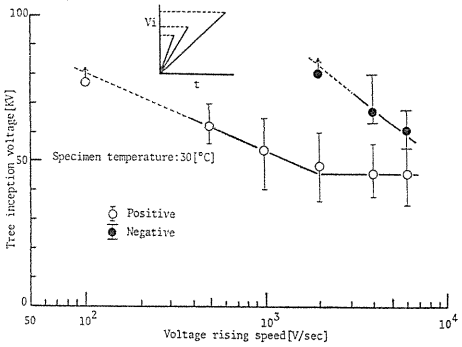

Fig. 37. Inception Voltage of dc tree as a function of voltage rising speed.

(2) *The Time for the Formation of a Stable Space Charge Distribution*

In order to identify the homo space charge accumulated near the needle electrode due to the dc prestress, the "short-circuit tree" was investigated. This tree is initiated by a strong electric field near the needle electrode which is induced by the accumulated space charge.

Several important factors affecting the space charge accumulation, such as the magnitude of the dc voltage, application period of the dc voltage, temperature of the specimen and the material of the needle electrode are discussed as well as these effects on the tree extension length. The extension is important in estimating the spatial distribution of the space charge, because it corresponds to the propagation of the local solid breakdown.

Fig. 38 shows the extention length of

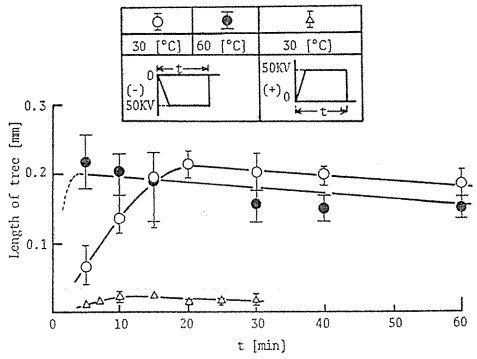

Fig. 38. Effect of duration of dc prestress on length of short-circuit tree.

the short-circuit tree as a function of the duration of a dc prestressing of 50kV. It is observed in Fig. 38 that the tree length for negative polarity at 30℃ increases untill the duration reaches 20 minutes, and then slowly decreases. At 60℃ the maximum is reached after only 5 minutes. These results show that a rather long period is required for the accumulation of a significant amount of negative space charge at 30℃. When a positive dc voltage is applied to accumulate the positive space charge, the extension length of the tree is much less than that of negative one. This is considered to be due to the difference between negative and positive space charge especially in the quantity and their spatial distribution.

(3) *Dependence of the Tree Extension Length on the Needle Electrode Material*

The amount of injected carriers from the electrode might be expected to affect the formation of the space chrge. In order to confirm this, the extension length of the tree was measured using three kinds of electrode metals (Ag, Fe, Pt) with the same radius of curvature of the needle tip. As shown in Fig. 39, the tree length for the negative prestress decreases with increasing work function of the metal electrode, which indicates clearly that the degree of carrier injection from the electrode has an influence on the space charge formation.

It should be mentioned that the tree length for the positive prestress is very small and almost independent of the electrode material.

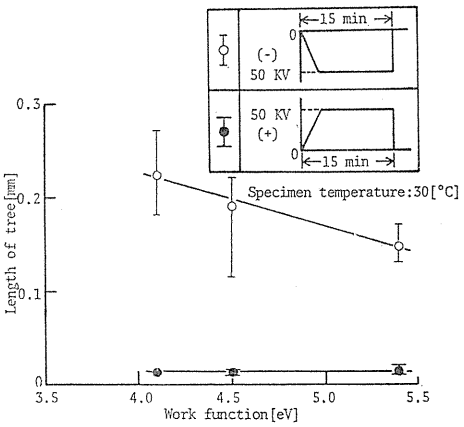

Fig. 39. Effect of electrode work function on length of short-circuit tree.

(4) *The Time for the Extinction of a Stable Space Charge Distribution*

The polarity reversal of dc voltage is one of the techniques used to reverse electric power flow along dc transmission. We must pay attention, therefore, to the influence of the polarity reversal on the distorted field distribution due to space charge accumulation in the insulation system.

In the previous section, it has been pointed out that treeing breakdown depends on the formation of a homo space charge associated with dc voltage application near the needle electrode. However, the homo space charge built up in the vicinity of the needle electrode disappears with time after removal of the voltage.

Figure 40 shows that the length of the porality-reversal tree decreases gradually as the rest time increases and that the space charge dissipation is different between different polarities. The length of the impulse tree is also plotted in Fig. 40. The rest times corresponding to these points are considered as the peried for which the space charges are dissipated about 50 min for negative space charge and about 1600 min for positive space charge. It is concluded from the rather long dissipation time that the carriers are captured in deep traps in pollyethylene and are not released readily at room temperature. The nature of the traps will be discussed later.

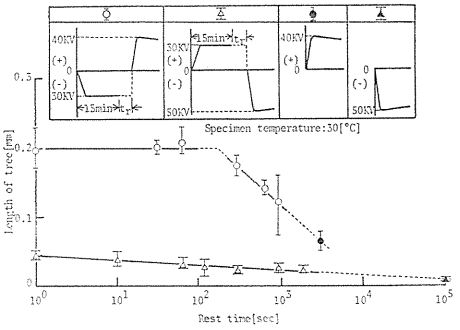

Fig. 40. Relationship between length of polarity reversal tree and rest time between application of dc and impulse voltages.

(5) *Temperature Dependence of Space Charge Distribution*

Figure 41 depicts the temperature dependence of the extension length of the polarity-reversal tree. The rest time for temperature characteristic was fixed at 1 sec. The length of the impulse tree is also plotted in this figure, being consistent with the intrinsic breakdown characteristic of PE as a function of temperature. As shown in the figure, the extension length of the polarity reversal trees almost coincide with those of the impulse trees in low temperature range, in spite of the extremely short rest time, indicating that the space charge effect apparently disappears. The effect of prestress on the tree lengths is observed above room temperature where the lengths of the polarity reversal trees are greater than those of the impulse trees. If it is assumed that, during a negative dc prestress, the number of injected electrons does not depend on temperature, then it can be inferred that the injected electrons are trapped in the extreme proximity of the needle tip or that the dissipation time of the trapped carriers is quite short (less than one second), that is, the carriers are trapped in very shallow levels or behave like free electrons. Further investigations are now being conducted to determine which of these two processes is actually taking place.

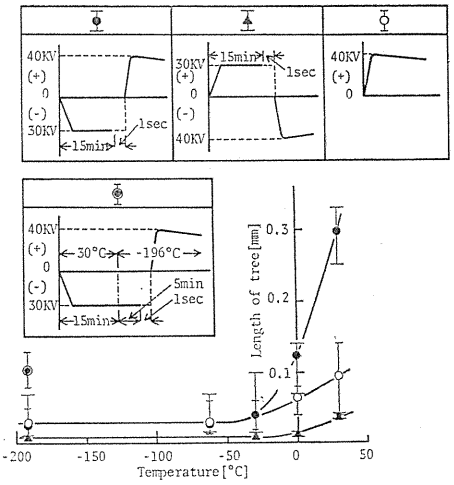

Fig. 41. Temperature dependence of length of polarity-reversal tree and impulse tree.

The mark ◉ in Fig. 41 shows the tree extension length for a specimen kept at liquid nitrogen temperature after electron injection due to the prestress of −30 kV for 15 minutes at 30℃. This fact indicates that the geometric pattern of space charge formed at 30℃ is still kept at the liquid nitrogen temperature and that the injected electrons travel over rather long distances until captured at deep trapping sites, without being captured at the shallow trapping sites because of their relatively large thermal energy at 30℃.

At the low temperature, the injected electrons can be captured at the shallow traps due to their relatively low thermal energy and the space chage formation will be expected to be located very closely to the needle electrode.

(6) *A Consideration of the Tree Initiation Mecanism*

In the previous subsections, some of the characteristics have been described of several kinds of trees associated with a homo space charge accumulation near the needle when dc voltage is applied. These phenomena are based on the partial breakdown of polyethylene caused by the high electric field existing near the needle electrode due to the space charge formed by the dc voltage.

The dependence of the tree inception voltage of a dc tree on the voltage rising rate can be understood qualitatively in the following way; the applied dc stress at the needle tip is relaxed by a homo space charge due to the carrier injection and extraction during the dc voltage application. The difference in the tree inception voltage with the polarities of the applied dc voltage might be partly based on the different degree between electron injection and extraction for negative and positive polarities, respectively.

The short-circuit tree is observed when the partial breakdown paths are produced at the instant of short-circuit by the inverse field set up by the space charge. The observed tree length can be taken as a measure of the spatial distribution of the space charge. To check this, the flight distance of the injected electron for a negative prestress has been estimated over which electrons injected from the needle electrode drift along the electric field until they are trapped. This flight distance λ is given by

$$\lambda = \mu \cdot \tau \cdot F \tag{11}$$

where μ is the electron mobility, τ is the life time of an electron and F is the electric field. Taking $\mu = 10^{-3}\mathrm{cm}^2/\mathrm{V}\cdot\mathrm{sec}$, $\tau = 10^{-6}\mathrm{sec}$ and $F = 5\mathrm{MV/cm}$[97], the value of the flight distance can be estimated at $\lambda = 50\mu\mathrm{m}$ which is of the same order as the tree extension length obtained experimentally. Taking the above fact and the effect of the voltage application time shown in Fig. 38 into consideration, the necessary amount of space charge might be considered to be formed through two processes; first, a homo carrier injection from the electrode and its trapping in the vicinity of the flight distance, and second, the accumlation of the injected carrier due to the successive voltage application, its self-diffusion and retrapping.

The complete dissipation time of the trapped carriers obtained from the polarity reversal tests above room temperature is quite long, which seems to indicate that the deep traps have a prominent influence. The effects of polarity and the lack of electrode material dependence of the tree length for a positive prestress indicate that the formation of a positive homo space charge is not due to hole injection but to the positive carriers left behind by electron extraction based on electron collision ionization in the high field region.

(7) *Carrier Trapping Sites Estimated from TSC and TL Techniques*

In the former sections, various dc treeing phenomena in polyethylene have been discussed based on a space charge formation caused by electron injection or extraction. It has been pointed out that with a negative voltage applied to the needle electrode, electrons injected from the electrode and captured at trapping sites with

different energy levels have an important effect of the space charge formation. To clarify the properties of electron traps, thermally stimulated current (TSC) and thermoluminescence (TL) techniques were applied to PE.[98]

The experimental procedure of TSC and TL are described below. First, the sample of about 30μm in thickness is cooled to a low temperature, T_1 (−185℃), in vacuum (10^{-3} Torr) and irradiated with x-rays for 20 min. in order to fill the traps with carriers. A bias voltage of 180V is then applied. The sample is heated at the rate of 6℃/min. from T_1 to a high temperature T_2 near the melting point of the crystalline regions. While the temperature is increasing, TSC and TL spectra are measured (1 st run). Next, the sample is cooled again to T_1 and re-heated with no x-ray irradiation under the same experimental conditions (2 nd run). The difference between the first and second TSC spectra is due to the release of trapped carriers. The second TSC spectrum has no trapped carriers.

Typical first and second TSC spectra together with TL spectrum are given in Fig. 42. The first TSC spectrum shows five TSC peaks designated P_1-P_5 in ascending order of temperature, whereas the second TSC is too small to detect any TSC peak except the steady conduction current above 50℃. Since the big difference between the two TSC spectra is due to trapped carriers, these five TSC peaks are concluded to be caused by the thermal release of trapped carriers. In Fig. 43, the trap depth obtained from the application of the partial heating method [99] is plotted against the maximum temperature reached in each partial heating.

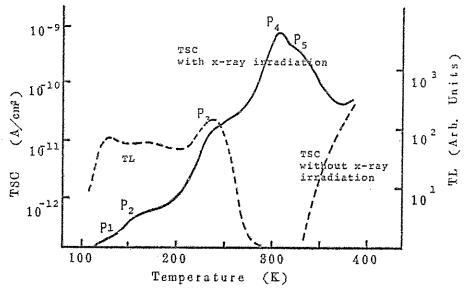

Fig. 42. TSC and TL spectra of LDPE.

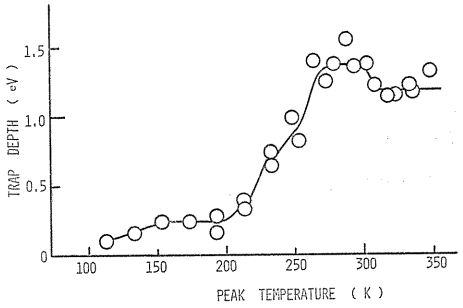

Fig. 43. Estimated trap depths of trapping centers by applying partial heating method to TSC.

Comparing the present results with the peak temperatures of the mechanical loss peaks by L. E. Nielsen,[100] the following assignments of the traps corresponding to each TSC peak are proposed:

P_2 (0.2e V); traps whose detrapping is enhanced by the γ-relaxation

P_3 (0.8 eV); traps in the amorphous regions whose detrapping is enhanced by the β-relaxation

P_4 (1.3 eV); traps in the boundary regions between the crystalline and the amorphous regions

P_5 (1.2 eV); traps in the crystalline region.

Although many uncertainties still remain about the origin of traps, cavity traps formed by the local arrangement of molecular chains are preferred to explain the results over to those caused by the carbonyl groups.[101]

The TL spectrum also supports these conclusions. As shown above, several trapping sites with different energy levels exist in LDPE, supporting our model mentioned above for the initiation of dc treeing breakdown.

(8) *Space Charge Evaluation by TSC method.*[102]

The authors have made clear till the previous subsections that the treeing breakdown starting from the vicinity of the tip of needle electrode inserted into polyethylene is considerably affected by the space charge.

Next, the nature and behavior of space charge accumlated in the specimen with a point-to-plane electrode arrangement will be discussed from the analysis of thermally stimulated current (TSC) under short-circuited condition.[102] Fig. 44 shows the typical TSC spectra in LDPE blended with the different contents of ionomer under a point-to-plane electrode system. Each curve exhibits one peak. With an increase of the ionomer content, the TSC peak temperature becomes higher and the magnitude decreases. It was also found that the TSC peak increases linearly with the increase of the forming voltage V_f. Figure 45 shows the relation

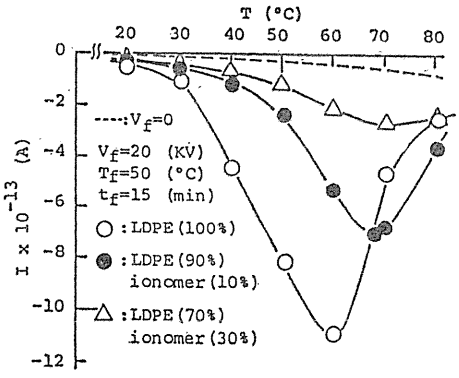

Fig. 44. Typical TSC spectra of ionomer blended PE.

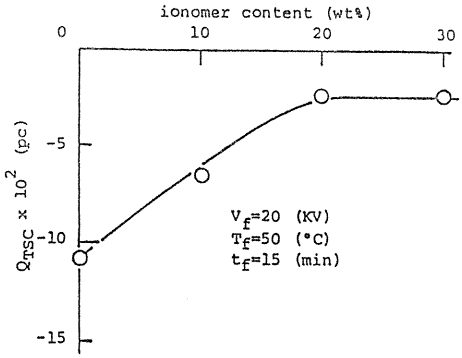

Fig. 45. Dependence of Q_{TSC} on ionomer content.

between the ionomer content and the total trapped charge Q_{TSC} calculated from the area of TSC spectra in ionomer blended LDPE. Q_{TSC} decreases with the increase of the ionomer content, and reaches a constant value above 20 Wt%. The space charge formation is suppressed by the ionomer in LDPE. The relation between the accumulated charge Q_{TSC} and dc tree inception voltage was investigated. It was found that the dc tree inception voltage decreases with the decrease of Q_{TSC}. This result suggests that the accumulated homo-space charge due to injected electrons moderates the electric field intensity near the tip of the needle electrode. The amount of accumulated space charge is suppressed by the blending of ionomer in LDPE.

3. 2. AC Treeing Breakdown

AC treeing breakdown is the important factor controlling the long time breakdown process of polymer insulating systems.

In spite of the extensive effort extended, there is still a lack of understanding

of its mechanism because of its complicated nature.

In this section, using experimental results obtained in our laboratory together with those presented by others, our considerations for the fundamental processes of ac treeing breakdown, limited to only electrical trees, will be reviewed by dividing them into two stages: tree inception and tree propagation.

3. 2. 1. A Phenomenological Consideration of AC Treeing Breakdown

Seccessive growth of partial degradation (treeing) to the complete puncture initiated from the tip of the point electrode with the curvature of 15 μm is given in Fig. 46 for repeated impulse voltage application on polymethyl methacrylate (PMMA) and PE of 2 mm thickness as a function of repeated cycles. Many investigations have shown that successive growth of degradation is caused from repeated gas discharges inside the tree channel with an order of one μm in diameter and an insulated internal wall. Assuming, for simplicity, Δd being mean length of degradation per one shot of impulse discharge and N its repeated cycles per second, the total degradated length per second is $\Delta d \cdot N$ and the total time $t = d/(\Delta d \cdot N)$ is requred to propagate the length d. As a source of energy to degradate a small portion Δd of polymer into the gaseous state and its conversion mechanism, there are two possible processes i) and ii), given in Table 12.

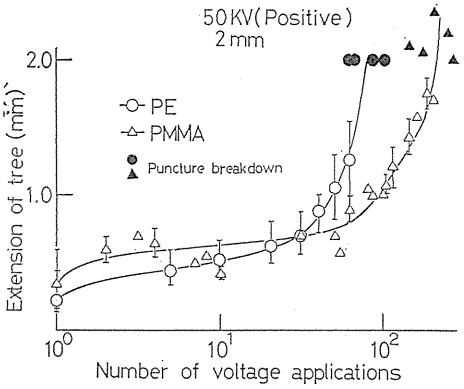

Fig. 46. Tree growth under repeated application of impulse voltage.

Table 12. Expected energy sources and their conversion mechanism for treeing breakdown due to gas discharge.

Process	Energy source	Energy conversion mechanism
i)	Discharge energy of gas	Bombardment of accelerated charge particles, chemical reaction of activated particles and thermal conduction etc.
ii)	Static energy of electric field	Solid dielectric breakdown

A typical partial breakdown path is observed even in inorganic glass with small cracks and melted spots.[103] The fact that treeing type electrical breakdown appears more easily in organic materials gives us an important suggestion that the process i) must be taken partly into consideration for tree propagation. A model of tree propagation which includes the process i) will be given later.

3. 2. 2. High Electric Stress Caused by Gaseous Discharge in Tree Channel and Induced Polymer Breakdown

Under the electrode arrangement as shown in Fig. 47, the potential of the

upper electrode is transferred on the polymer surface through the plasma colum of gas discharge and a high electric stress is induced on it, depending upon the potential drop and diameter of the plasma column. The diameter of the plasma has a close relation with the gas density and its electron affinity since it is roughly determined by the transverse diffusion. Thus, different effects among electric discharges in air, SF_6 and oil will be expected on the partial dielectric breakdown of polymer associated with these media. The author has summarized for the electrical breakdown of PE film following a single burst of partial discharges in air and oil[104] that:

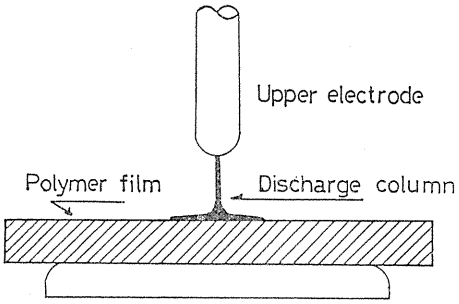

Fig. 47. Electrode arrangement of polymer film breakdown caused by gas discharge.

a) Fundamentally, the breakdown strength of PE under the above condition is nearly the same as that under a metal to metal electrode arrangement.

b) The aparent F_B of PE depends upon the diameter of the discharge column.

c) The polarity effect of F_B is due to different space charge formation.

Next, let us consider the nature of induced high electric stress from the point of view of the time base. The pulsed nature of dc gas discharges at the negative point has been well understood as the Trichel pulse, which is formed by the appearance and disappearance of the effective retardation field of negative ionic space charges. As shown in Fig. 47, accumulation of homo charges on the PE film extinguishes gas discharge because of the reduced electric field in the gas space. Therefore, a sustained period of gas discharge is restricted below about 0.1 μsec. Under dc and voltage with a small value of voltage inclination, dV/dt, induced electric stress on the solid surface has a pulsed and a strong non-uniform nature.

In the case of ac voltage application, a series of discharge pulses occur at the different phase angles over one cycle of the voltage wave form. A different effect by each pulse should be expected on the partial breakdown because the potential drop across PE film differs for each discharge pulse occurring at a different phase angle. This is the main reason why the voltage acceleration test is not preferred for treeing breakdown. If the chemical erosion by gas discharge were to play an important role for the tree propagation, then the voltage acceleration test could be applied with good results, since the discharge energy of each pulse would be expected to be nearly the same.

3. 2. 3. Inception of tree Channel

(1) *Voltage and Temperature Dependence of Induction Period*

The tree inception is defined here as that point when a tree channel observed under an optical microscope attains a length of 20 μm along the axis of the needle electrode.

When an applied electric stress over a given extent of distance from the needle tip exceeds the breakdown strength of the polymer, the partical electrical breakdown will be expected to occur with a rather small time lag after voltage application, and then the tree channel is formed. Figure 48 shows the calculated electric

stresses F_{inc} at the needle tip when the initial tree starts, as a function of d/r where d being the gap spacing and r the radius of curvature of the needle tip. These calculated electric stresses roughly correspond to the intrinsic electric strength of PMMA and their polarity and d/r dependences are understood from the space charge effect around the needle point.

On the other hand, the channel can be initiated at a given time after voltage application less than the breakdown stress without any observable gas discharge above 1 pC. The existence of such an induction period may give an important suggestion for the tree inception process. In Fig. 49 induction periods obtained for PE are given as a function of the ac voltage and temperature.

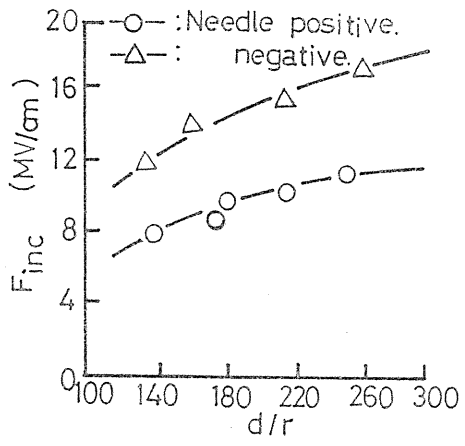

Fig. 48. Electric stress (F_{inc}) at the needle point when tree initiates as a function of d/r under impulse voltage application in PMMA.

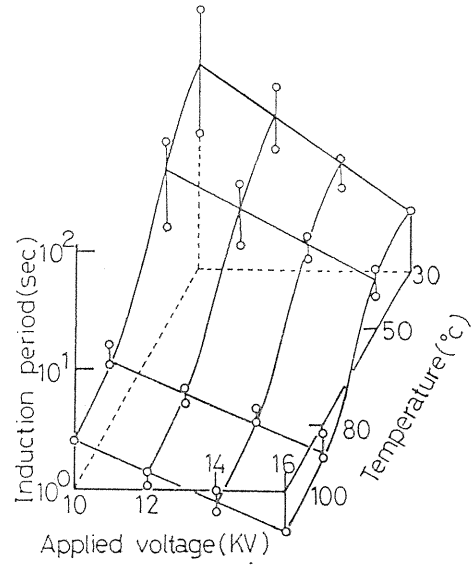

Fig. 49. Induction period for tree initiation as a function of applied voltage and temperature in PE.

(2) *A model of Tree Inception*

In the case of $F_{appl}>F_i$ (intrinsic electric strength), the tree channel is initiated due to the pure partial electrical breakdown of the polymer. On the other hand, under the condition of $F_{appl}<F_i$ the tree channel might be initiated with an induction period. As to the inception process of treeing, Yoda et al.[105] suggested that a bud of the tree is caused by the interaction between high energy electrons accelerated by electric field and the end radicals of polymer structure, and Yamada[106] considered that it was due to a fatigue breakdown owing to a Maxwell mechanical stress associated with repeated voltage application.

From experimental results mentioned above, the author presents a model as shown in Fig. 50, which considers the fact that a crazing phenomenon requires an induction period for its appearance which strongly depends on amounts of mechanical stress and temperature of polymer[107~109] as the case of tree initiation. A repeated electro-mechanical stress induced around the needle point by ac voltage application works as a compression force on the polymer. Then, the induced

mechanical stress perpendicular to the direction of the electric field appears in an elastic material such as a polymer by which the crazing might be caused starting from a micro-defect such as a micro-void in the polymer when the stress exceeds a critical value. As a second stage, the crazing grows into a void-crack. Thus, the time to appearance of void-cracks by way of crazing seems to correspond to the induction period of tree inception. Of course, we can also recognize a model by Yoda et al[105] as one of possible processes to initiate a tree channel.

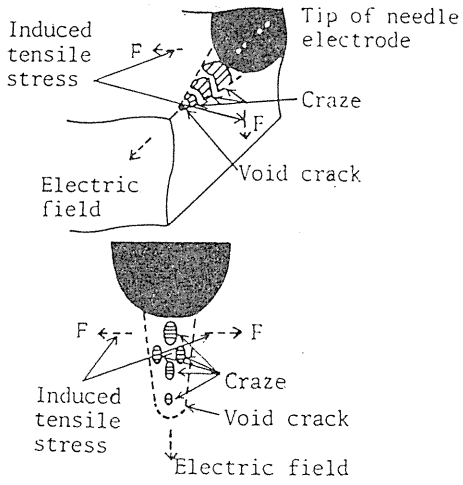

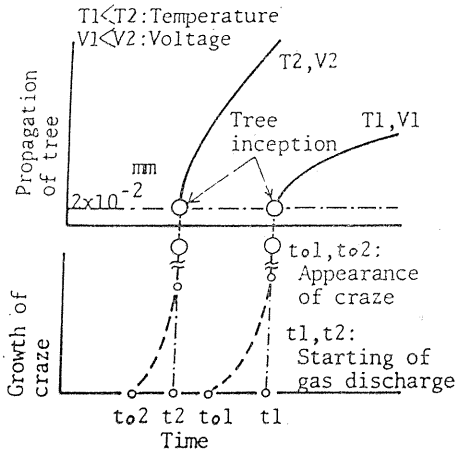

Fig. 50. Model for tree initiation.

3. 2. 4. Propagation of Tree Channel

(1) *Tree Shapes and Propagation of Tree Channel*

After the tree inception, the tree channel starts to extend its length due to gas discharges repeated in it, but its propagation behavior depends upon wave form and magnitude of applied voltage, kind of polymer and its temperature etc. These results in patterns of tree shape which are generally divided into three kinds; tree-like, bush-like and fan-like as shown in Fig. 51. Figure 52 shows a tree propagation behavior in PE at various temperatures as a function of time after the voltage application. As seen in this figure, the tree propagation process has to be discussed by taking the tree shape into consideration. At 30℃, for instance, tree shapes at 10 and 12 kV are tree-like, while those at 14 and 16 kV change from tree-like at the initial stage to bush-like as time elapses. Tree shape and its propagation depend on the gas pressure of decomposed molecules inside the tree channel, which in turn controls the nature of gas discharge at the following stage. Increased pressure inhibits the firing of discharge in the tree channel and the new

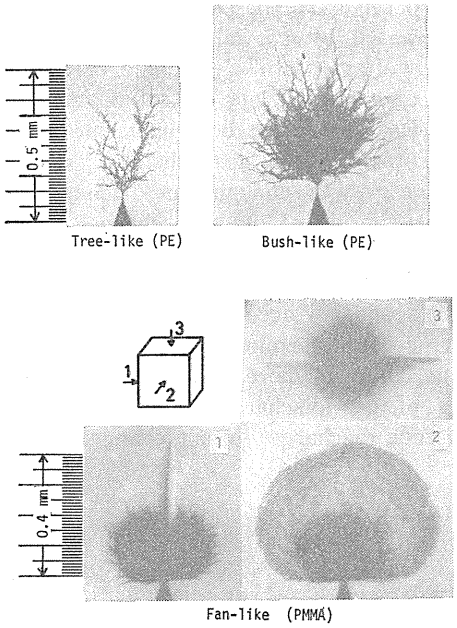

Fig. 51. Various patterns of tree shape.

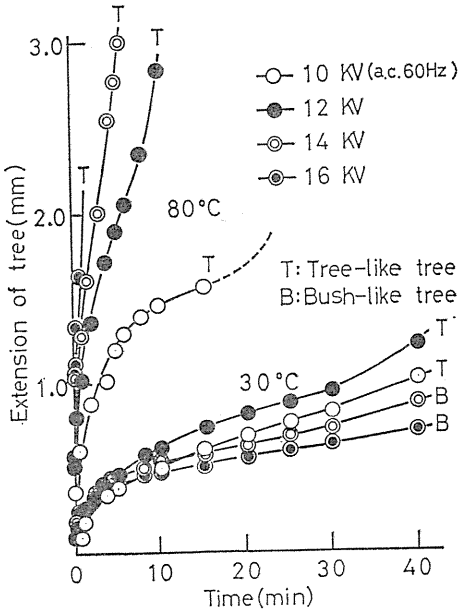

Fig. 52. Tree growth as a function of time after voltage application in PE.

tree channel may be formed in some other direction. This is the reason for the appearance of the bush-like tree with many branches. If leakage of decomposed gases is allowed, the tree channel starts again to extend from one of the bush-like channels. At 80℃, the tree shape remains tree-like without changing its shape into bush-like until complete puncture of the polymer takes place for all specimens at four kinds of applied voltage tested, because the gas pressure inside the tree channel is reduced by increased gas diffusion and absorption rates at this high temperature. The fan-like pattern is sometimes observed in a brittle polymer such as PMMA.

(2) *A Model of Tree Propagation*

Experimental results mentioned above together with those of electrical properties of gas discharge are summarized on tree propagation as follows:

a) Tree propagation is induced by internal gas discharge in the tree.

b) Gas discharge is pulsive, the duration of which is below 0.1 μsec.

c) The velocity of the partial extension of a tree channel during one shot of a pulse discharge is of the order of 10^5cm/sec.[110, 111]

d) The electric potential of the needle electrode is transferred to the tip of the old tree channel through the conductive plasma of gas discharge.

e) F_B of the polymer film determined under two different electrode conditions, one is using metal to metal electrodes and the other using a plasma column of gas discharge as one of electrode, are found to be nearly equivalent.

f) The diameter of the tree channel is of the order of μm and is expanded gradually by repeated gas discharges.

The model of tree propagation which is proposed from the above considerations is that the propagation of the tree channel is caused by partial electrical breakdown of the polymer under the impulse-like voltage with a strongly divergent electric field induced by the conductive plasma of gas discharge. Electron avalanche, impulse thermal or impulse mechanical breakdown might be responsible for a basic process of tree propagation, depending on the physical and chemical nature of the polymer. In order to produce a new tree growth, enough gas discharge is required to produce a high electric stress at the tip of old tree channel. The chemical erosion process helps to introduce such a powerful gas discharge in the old channel diameter. It should also be noted that the voltage acceleration test for treeing is not preferred compared with the frequency acceleration test, because the voltage phase when the gas discharge just occurs determines the magnitude of the local electric stress at the tip of discharge column, whereas in the frequency acceleration test only the repeated numbers of gas discharge increases, but the phase relation with voltage for appearance of each discharge doesn't change.

4. Conclusion

Electrical breakdown of various kinds of polymers has been discussed on the basis of various results obtained in our laboratoly along with those by many investigators. As have been shown, the electrical breakdown phenomena of polymers are very sensitive to their physical and chemical natures. Further work on the breakdown mechanism of polymers should be carried out with a clearer characterization of polymer structure.

Acknowledgement

We are deeply grateful to Professor Goro Sawa of Mie University for his helpful suggestions and stimulating discussion. Especially, in preparing this paper, a critical reading of the manuscript was carried out by Professer Sawa. We also express our great appreciation to Professor Masato Nawata of Meijo University, Assistant Professor Keiichi Miyairi of Shinshu University, Lecturer Hideaki Kawamura of Meijo University, Assistant Professor Keiichi Kitagawa of Gifu Technical College, and Lecturer Masayuki Nagao of Toyohashi University of Technology for their considerable cooperation in the experiment and helpful discussion. Their contributions to this paper are very great and we take pleasure in acknowledging the important part played by them.

This work was supported by the Grant in Aid for Scientific Research from the Ministry of Education of Japan.

References

1) M. Ieda; IEEE Trans. **EI-15** (1980) 206.
2) S. Whitehead; "Dielectric Breakdown of Solids" Clarendon Press, Oxfod (1953).
3) J. J. O'Dwyer; "The Theory of Electrical Conduction and Breakdown in Solid Dielectrics" Clarendon Press, Oxford (1973).

4) M. Ieda, G. Sawa and N. Nagao; Internationals Symposium Hochspannungstechnik, Zürich, 5. 1-04 (1975) 587.
5) A. E. W. Austen and H. Pelzer; J. Inst. Elect. Engrs. **93**(I) (1946) 525.
6) J. J. Mckeown; Proc. Inst. Elect. Engrs. **112** (1965) 824.
7) P. H. H. Fischer and K. W. Nissen; IEEE Trans. EI-11 (1976) 37.
8) D. W. Watson; IEEE Trans. EI-8 (1973) 6.
9) I. D. E. Bail; Proc. Inst. Elect. Engrs. **98**(I) (1951) 84.
10) W. G. Oakes; J. Inst. Elect. Engrs. **95**(I) (1948) 36.
11) W. G. Oakes; J. Inst. Elect. Engrs. **96**(I) (1949) 37.
12) J. Artbauer and J. Griac; Acta Technica CSAV (1966) 416.
13) K. Amakawa, T. Moriuchi, T. Yoshida and Y. Inuishi; J. Inst. Elect. Engrs. of Japan **84** (1964) 129.
14) J. M. Meek and J. D. Craggs; "Electrical Breakdown of Gases" John Wiley & Sons, New York (1978).
15) I. Kitani and K. Arii; Trans. Inst. Elect. Engrs. of Japan **94**-A (1974) 251.
16) K. W. Wargner; AIEE Trans. **41** (1922) 288.
17) W. Rogowski; Arch. Elektrotech. **19** (1930) 569.
18) A. von Hippel; J. Appl. Phys. 8 (1937) 815.
19) Y. Inuishi, K. Onishi, Y. Tada and N. Suita; J. Inst. Elect. Engrs. of Japan **76** (1956) 913.
20) J. Artbauer and J. Griac; Proc. Inst. Elect. Engrs. **112** (1965) 818.
21) H. Fröhlich; Proc. Roy. Soc. A-188 (1947) 521.
22) K. H. Stark and C. G. Garton; Nature **176** (1955) 1225.
23) J. Artbauer; Kolloid Z. und Z. Polymere **202** (1965) 15.
24) H. J, Wintle; J. Appl. Phys. **52** (1981) 4181.
25) P. H. Moon; Trans. Am. Inst. Elect. Engrs. **50** (1931) 1008.
26) N. Klein; Adv. Electron, Electron Phys. **26** (1969) 309.
27) M. Hikita, M. Ieda and G. Sawa; J. Appl. Phys. **54** (1983) 2025.
28) J. Vermeer; Physica **22** (1956) 1269.
29) K. Miyairi, G. Sawa and M. Ieda; Electrical Engineering in Japan **92** (1972) 21.
30) M. Hikita, M. Nagao, G. Sawa and M. Ieda; J. Phys, D; Appl. Phys. **13** (1980) 661.
31) M. Hikita, M. Nagao, G. Sawa and M. Ieda; J. Phys. D; Appl. Phys. Letters to the Editor. **16** (1983) L157.
32) K. Miyairi; Trans. Inst. Elect. Engrs. of Japan **103**-A (1983) 203.
33) J. J. O'Dwyer; 1981 Annual Report on Conference of Electrical Insulation and Dielectric Phenomena (1981) 193.
34) C. Copple, D. R. Hartree, A. Porter, and H. Tyson; J. Inst. Elect. Engrs. **85** (1939) 56.
35) M. Hikita, M. Nagao, G. Sawa and M. Ieda; Trans. Inst. Elect. Engrs. of Japan **101**-A (1981) 489.
36) M. Ieda, M. Hikita, M. Nagao and G. Sawa; 1982 Annual Report on Conerence of Electrical Insulation and Dielectric Phenomena (1982) 444.
37) M. Nagao, G. Sawa and M. Ieda; Trans. Inst. Elect. Engrs. of Japan **96**-A (1976) 605.
38) M. Nagao, S. Toyoshima, G. Sawa and M. Ieda; Trans. Inst. Elect. Engrs. of Japan **97**-A (1977) 617.
39) K. Amakawa and Y. Inuishi; Japan. J. Appl. Phys. **12** (1973) 755.
40) M. Nagao, G. Sawa and M. Ieda; Japan. J. Appl. Phys. **15** (1976) 547.
41) M. Ieda, Y. Takai, M. Nagao and G. Sawa; Dielectric Materials, Measurements and Applications, Conf. Publ. No. 129 (Inst. of Elect Engrs., London, 1975) 249.
42) K. Miyairi, T. Yamauchi, G. Sawa and M. Ieda; J. Inst. Elect. Engrs. of Japan **91** (1971) 1962.
43) I. O. Salyer and A. S. Kenyon; J. Polymer Sci. A-**19** (1971) 3083.
44) W. G. Lawson; Proc. Inst. Elect. Engrs. **113** (1966) 197.
45) H. Miyauchi and K. Yahagi; Trans. Inst. Elect. Engrs. of Japan **92**-A (1972) 36.
46) M. Ieda and G. Sawa; Japan Soc. Appl. Phys. **48** (1979) 1177.

47) S. N. Kolesov; IEEE Trans. EI-15 (1980) 382.
48) K. Kitagawa, G. Sawa and M. Ieda; Japan. J. Appl. Phys. **20** (1981) 87.
49) K. Kitagawa, G. Sawa and M. Ieda; Japan. J. Appl. Phys. **19** (1980) 389.
50) K. Kitagawa, G. Sawa and M. Ieda; Japan. J. Appl. Phys. **21** (1982) 1117.
51) K. Yahagi; IEEE Trans. EI-15 (1980) 241.
52) K. Yahagi and S. Katakai; 1 st International Conference on Conduction and Breakdown in Solid Dielectrics (1983) 345.
53) K. Yahagi and S. Katagai; Japan Soc. Appl. Phys. **52** (1983) 494.
54) S. Mita and K. Yahagi; Japan. J. Appl. Phys. **14** (1975) 197.
55) Y. Maeda and K. Yahagi; Japan. J. Appl. Phys. **16** (1977) 179.
56) M. Ieda, K. Kitagawa and G. Sawa; 1st International Conference on Conduction and Breakdown in Solid Dierectrics (1983) 333.
57) M. Hikita, S. Tajima, I. Ishino, G. Sawa and M. Ieda; Japan. J. Appl. Phys. (1984) 〔to be published〕.
58) H. Luy and F. Oswald; ETZ-A **92** (1972) 358.
59) K. Yoshino, H. Harada, J. Kyokane and Y. Inuishi; Japan. J. Appl. Phys. 18 (1979) 679.
60) K. Yoshino, H. Harada, J. Kyokane and Y. Inuishi; J. Phys. D: Appl. Phys. **12** (1979) 1535.
61) H. Wagner; 1974 Annual Report Conf. on Electrical Insulation and Dielectric Phenomena (1975) 62.
62) G. Sawa, K. Arakawa, M. Nagao and M. Ieda; Thin Solid Films **59** (1979) 131.
63) K. Kitagawa, G. Sawa and M. Ieda; Trans. Inst. Elect. Engrs. of **103**-A (1983) 150.
64) A. Low, D. Vesely, P. Allan and M. Bevis; J. Mater. Sci. **13** (1978) 711.
65) K. Miyairi and T. Yamada; Japan. J. Appl. Phys. **16** (1977) 1449.
66) K. Yahagi, A. Okinaka and S. Katakai; IEEE Trans. EI-18 (1983) 138.
67) S. Pélissou, H. St. Onge and M. R. Wertheimer; 1st International Conf. on Conduction and Breakdown in Solid Dielectric. (1983) 339.
68) K. Miyairi, G. Sawa and M. Ieda; Trans. Inst. Elect. Engrs. of Japan **92**-A (1972) 531.
69) Marushige, Takai, Saito and Ninomiya; Jour. of Industrial Chemistry **69** (1966) 1306.
70) N. W. Todd; Engineering (1964) 1026.
71) H. Yoshioka; J. Inst. Elect. Engrs. of Japan 87 (1967) 829.
72) M. Nagao, G. Sawa, M. Fukui and M. Ieda; Japan. J. Appl. Phys. **15** (1976) 1813.
73) M. Nagao, G. Sawa and M. Ieda; Trans. Inst. Elect. Engrs. of Japan **97**-A (1977) 279.
74) M. Ieda, M. Hikita and G. Sawa; 3rd International Symposium on High Voltage Engineering (1979) 21.05.
75) M. Hikita, M. Nagao, G. Sawa and M. Ieda; Trans. Inst. Elect. Engrs. of Japan **102**-A (1982) 309.
76) E. Sacher; 1976 Annual Report Confrence on Electrical Insulation and Dielectric Phenomena NAS (1976) 33.
77) K. Iida, S. NakaMura, M. Ieda and G. Sawa; Trans. Inst. Elect. Engrs. of Japan **103**-A (1983) 111.
78) L. J. Bellamy; "The Infra-Red Spectra of Complex Molecules" New York, John Will & Sons, Inc. (1953) 203.
79) J. Nishizaki; J. Chem. Soc. Japan, Ind. Chem. Sec. **69** (1966) 1393.
80) G. Pfister, Abkowitz and R. G. Crystal; J. Appl. Phys. **44** (1973) 2064.
81) Parker; NASA Rep. CR 124926 (1976).
82) R. Hasegawa, M. Kobayashi and H. Tadokoro; Polymer J. **3** (1972) 591.
83) Y. Wada and R. Hayakawa; Japan. J. Appl. Phys. **15** (1976) 2041.
84) S. Osaki, S. Uemura and Y. Ishida; J. Polymer Sci. **9** (1971) 585.
85) M. Hikita, M. Nagao, G. Sawa and M. Ieda; Trans. Inst. Elect. Engrs. Japan **101**-A (1981) 95.
86) D. C. Allam and C. T. H. Stoddart; Chemistry in Britain **2** (1965) 410.
87) H. Carchano, R.I acoste and Y. Segui; Appl. Phys. Lett. **19** (1971) 414.
88) Y. Segui, B. Ai and H. Carchano; J. Appl. Phys. **47** (1976) 140.

89) M. Ieda, M. Hikita, A. Matsuda, M. Nagao and G. Sawa; 1981 Annual Report on Conf. on Electrical Insulation and Dielectric Phenomena (1981) 207.
90) M. Hikita, A. Matsuda, M. Nagao, G. Sawa and M. Ieda; Japan. J. Appl. Phys. **21** (1982) 475.
91) M. Hikita, A. Matsuda, M. Nagao, G. Sawa and M. Ieda; Japan. J. Appl. Phys. **21** (1982) 483.
92) T. Mizutani, Y. Takai, T, Osawa and M. Ieda; J. Phys. D. Appl. Phys. **9** (1976) 2253.
93) R. H. Fowler and L. Nordheim; Proc. Roy. Soc. **A119** (1928) 173.
94) J. J. O'Dwyer; IEEE Trans. **EI-15** (1980) 264.
95) A. Bradwell, R. Cooper and B. Varlow; Proc. Inst. Elect. Engrs. **118** (1971) 247.
96) M. Ieda and M. Nawata; IEEE Trans. **EI-12** (1977) 19.
97) E. H. Martin and J. Hirsch; Solid State Commun. **7** (1969) 279.
98) T. Mizutani, Y. Suzuoki and M. Ieda; J. Appl. Phys. **48** (1977) 2408.
99) R. A. Creswell and M. M. Perlman; J. Appl. Phys. **41** (1970) 2365.
100) L. E. Nielsen; J. Polymer Sci. **42** (1960) 357.
101) Y. Suzuoki, K. Yasuda, T. Mizutani and M. Ieda; J. Phys. D: Appl. Phys. **10** (1977) 1985.
102) M. Nawata, H. Kawamura and M. Ieda; 4th International Symposium on High Voltage Engineering (1983) 22.02.
103) U. Shinohara; Memo. of Hokkaido Univ. **3** (1934) 157.
104) M. Ieda, G. Sawa, K. Miyairi and U. Shinohara; Conf. on Diele. Mat. Meas. and Appl., Lancaster (1970) 254.
105) B. Yoda and N. Sakabe; Hitachi Rev. **51** (1969) 72.
106) Y. Yamada; Sumitomo Electric Rev. **101** (1969) 24.
107) B. Maxwell and L. F. Rahm; Ind. Engng. Chem. **41** (1949) 1988.
108) D. K. Spurr and W. D. Niegisch; J. Appl. Polymer Sci. **6** (1962) 585.
109) J. C. Devins and C. W. Reed; 1970 Annual Rept. Conference on Electrical Insulation and Dielectric Phenomena (1970) 86.
110) B. Bittmer; Arch. für Elect. **48** (1964) 387.
111) B. Bolton; Conf. on Diel. Mat., Meas. and Appl., Lancaster (1970) 85.